Cell Stem Cell

Article

# Tunable differentiation of human CD4$^+$ and CD8$^+$ T cells from pluripotent stem cells

## Graphical abstract

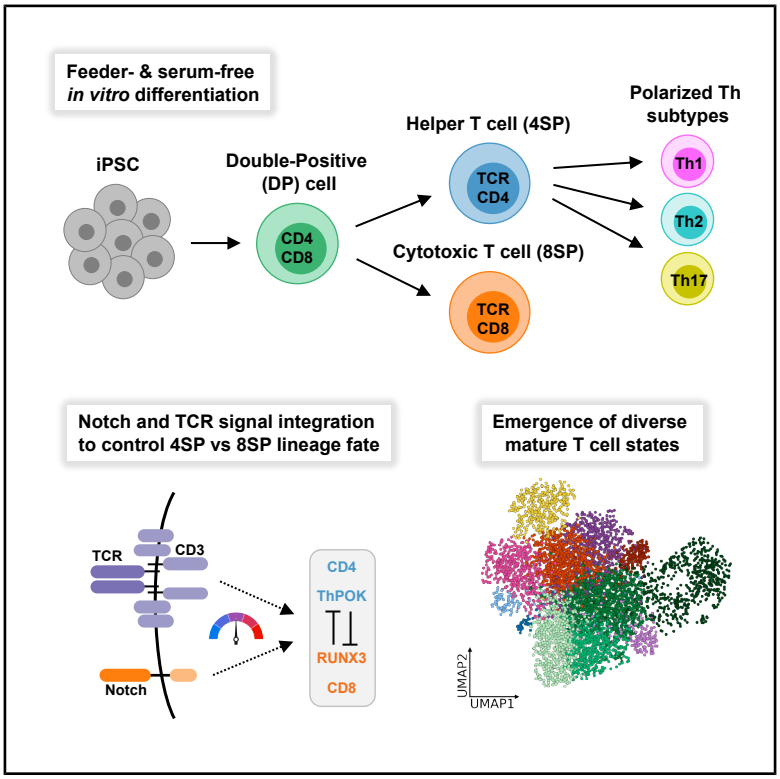


## Authors

Ross D. Jones, Kevin Salim, Laura N. Stankiewicz, ..., Fabio M.V. Rossi, Megan K. Levings, Peter W. Zandstra

## Correspondence

mlevings@bcchr.ca (M.K.L.), peter.zandstra@ubc.ca (P.W.Z.)

## In brief

Jones et al. demonstrate that Notch signaling suppresses CD4$^+$ (helper) T cell induction from PSCs and that manipulating TCR and Notch signaling enables control over CD4$^+$ vs. CD8$^+$ (cytotoxic) T cell production. The resulting PSC-CD4$^+$ T cells achieve a naive/memory phenotype and are capable of functional Th1/2/17 polarization.

## Highlights

- Notch suppresses *in vitro* production of CD4$^+$ T cells from PSCs
- Notch represses TCR signaling outputs, including the CD4 lineage factor ThPOK
- PSC-CD4$^+$ T cells express naive/memory T cell markers and diverse TCRs
- PSC-CD4$^+$ T cells express co-stimulatory receptors and can polarize *in vitro*

Jones et al., 2026, Cell Stem Cell *33*, 73–90
January 8, 2026 
https://doi.org/10.1016/j.stem.2025.12.010

CellPress

Cell Stem Cell

CellPress
OPEN ACCESS

Article

# Tunable differentiation of human CD4$^+$ and CD8$^+$ T cells from pluripotent stem cells

Ross D. Jones,[1,2,10] Kevin Salim,[3,4,10] Laura N. Stankiewicz,[1,2] John M. Edgar,[1,2] Lorna Leon,[3,4] Jana K. Gillies,[3,4] Ali Murtaza,[2,5,6] Lauren J. Durland,[1,2] Divy Raval,[1,2] Charles Lau,[1,2] Thristan Paulo B. Taberna,[1,2] Han Hsuan Hsu,[1,2] Carla Zimmerman,[1,2] Yale S. Michaels,[1,2,7,8] Fabio M.V. Rossi,[1,9] Megan K. Levings,[1,3,4,*] and Peter W. Zandstra[1,2,9,11,*]

[1]School of Biomedical Engineering, The University of British Columbia, Vancouver, BC, Canada
[2]Michael Smith Laboratories, The University of British Columbia, Vancouver, BC, Canada
[3]BC Children's Hospital Research Institute, Vancouver, BC, Canada
[4]Department of Surgery, The University of British Columbia, Vancouver, BC, Canada
[5]Department of Biology, The University of British Columbia, Vancouver, BC, Canada
[6]Synthetic Biology Institute, Rice University, Houston, TX, USA
[7]CancerCare Manitoba, Winnipeg, MB, Canada
[8]Department of Biochemistry and Medical Genetics, University of Manitoba, Winnipeg, MB, Canada
[9]Department of Medical Genetics, University of British Columbia, Vancouver, BC, Canada
[10]These authors contributed equally
[11]Lead contact
*Correspondence: mlevings@bcchr.ca (M.K.L.), peter.zandstra@ubc.ca (P.W.Z.)
https://doi.org/10.1016/j.stem.2025.12.010

## SUMMARY

Allogeneic T cell therapies are a highly desirable option to circumvent the cost and complexity of using autologous T cells to treat diseases. Allogeneic CD8$^+$ T cells can be made from pluripotent stem cells (PSCs), but deriving CD4$^+$ T cells from PSCs has remained a significant challenge. Using feeder- and serum-free conditions, we found that CD4$^+$ vs. CD8$^+$ T cell commitment from PSCs can be controlled by fine-tuning the dynamics of Notch and T cell receptor (TCR) signaling delivered to CD4$^+$CD8$^+$ double-positive T cells. Notch signaling negatively impacts CD4$^+$ T cell commitment, and its timed removal allows generation of clonally diverse and expandable CD4$^+$ T cells from PSCs. The resulting CD4$^+$ T cells respond to cytokine-mediated polarization by differentiating into Th1, Th2, or Th17 cells, recapitulating canonical helper cell function. These findings represent a significant step toward using PSC-derived CD4$^+$ T cells as a low-cost, off-the-shelf cell therapy.

## INTRODUCTION

Engineered T cells have an enormous potential to treat cancer, autoimmunity, and infectious disease.[1–3] However, the high cost and logistical complexity of manufacturing and administering autologous (patient-derived) T cells significantly limit access to T cell therapies. There has therefore been strong interest in the scalable, cost-effective production of allogeneic (off-the-shelf) T cells.[4–6] A promising source of allogeneic T cells is human pluripotent stem cells (PSCs), which are capable of indefinite expansion and more amenable to genetic engineering than primary cells and can be differentiated *in vitro* to cytotoxic (CD8$^+$) T cells.[7–10] Recently, we and others identified clinically relevant, fully defined (feeder- and serum-free) conditions to differentiate PSCs into CD8$^+$ T cells.[11–14] However, a long-standing challenge for PSC-to-T cell manufacturing, especially in feeder-free systems, has been the inability to make substantial numbers of mature helper (CD4$^+$) T cells.[6]

CD4$^+$ T cells play an essential role in "helping" CD8$^+$ T cells to eliminate cancer in the context of both engineered T cell therapies[15–18] and immunotherapies.[19–23] Moreover, through their ability to differentiate into different helper T (Th) cell subsets, such as Th1, Th2, and Th17 cells, CD4$^+$ T cells orchestrate and regulate diverse immune responses.

*In vivo* differentiation of CD4$^+$ vs. CD8$^+$ T cells is driven by the dynamics of T cell receptor (TCR) signaling.[24,25] In the thymus, T cell progenitors develop into double-positive (DP) CD4$^+$CD8$^+$ cells and then undergo V(D)J recombination and positive and negative selection. The resulting cells have functional TCRs that interact with CD4 or CD8 co-receptors and recognize peptide-loaded major histocompatibility complex (pMHC) class I (CD8$^+$ T cells) or class II (CD4$^+$ T cells) proteins. Commitment to the CD4 or CD8 lineage is controlled by TCR signaling duration[26,27]; in positively selecting thymocytes, TCR-pMHC interactions induce transient CD8 downregulation, interrupting interactions with MHC class I and leading to shorter signaling outputs by class I-reactive TCRs.[24,25] Differences in TCR signaling dynamics lead to selective activation of RUNX3 (CD8) or ThPOK (*ZBTB7B*, CD4), which are mutually repressive lineage-defining transcription factors (TFs).[28–30]

An outstanding question is why current PSC-to-T cell differentiation protocols lead to poor CD4$^+$ T cell development. We hypothesized that suboptimal TCR stimulation led to a strong bias toward CD8$^+$ T cells. Of particular interest were effects of Notch signaling, a pathway crucial to T cell development and known to have dose-dependent effects on TCR signaling and CD8$^+$ T cell development.[31,32] Notably, in a study using artificial thymic organoids (ATOs) to produce T cells from PSCs,[33] more CD4$^+$ T cells developed when using MS5 feeder cells expressing the Notch ligand delta-like ligand 1 (DLL1) rather than the stronger ligand DLL4.[34] We thus studied the combined effects of Notch and TCR signaling levels on *in vitro* differentiation of PSCs to CD4$^+$ vs. CD8$^+$ T cells.

## RESULTS

### Notch signaling suppresses production of CD4$^+$ T cells from PSCs

*In vitro* production of T cells from PSCs is a multi-stage, ~6- to 8-week process that replicates key aspects of *in vivo* T cell development[13,35] (Figures 1A, 1B, S1A, and S1B). Since TCR signaling strength and duration are key determinants of CD4$^+$ vs. CD8$^+$ T cell commitment, we first tested the effects of different levels of TCR stimulation on CD4$^+$ T cell differentiation from the iPS11 induced pluripotent stem cell (iPSC) line (ALSTEM). After generating iPSC-DP cells as previously described,[13] cells were treated with different levels of soluble anti-CD2/3/28 TCR-stimulating complexes and re-plated onto fresh DLL4 (10 μg/mL) + VCAM1 (2.5 μg/mL) (Figure 1C). Although we hypothesized that more TCR-stimulating input would increase CD4$^+$CD8$^-$ (CD4 single-positive, 4SP) cell formation,[26] we were surprised to find that high levels favored CD4$^-$CD8$^+$ (CD8 single-positive, 8SP) cells while a small population of 4SP cells was only observed at lower levels (Figure 1C). Among cells expressing CD27, a marker of lineage commitment and maturation[36] (Figure S1C), the maximal percent and yield of 4SP cells were between ~0.1% and 0.3% anti-CD2/3/28 (Figure 1C, lower), so we used this range for further optimization.

We next examined the effect of Notch signaling on iPSC-DP-to-SP induction. In the neonatal thymus, Notch ligand densities are highest in the cortical-medullary junction and outer cortex, with diminishing density in the inner cortex, the site of positive selection—especially for DLL4, the most potent ligand[37] (Figure 1D). To test if Notch signaling affects iPSC-CD4$^+$ T cell formation, we repeated the above with 0.1% anti-CD2/3/28 while inhibiting Notch using the gamma secretase inhibitor (GSI) DAPT. DAPT caused a striking dose-dependent switch from 8SP to 4SP cell induction in terms of both cell ratios and yields (Figures 1E and 1F), suggesting that Notch signaling biases *in vitro* PSC-to-T cell differentiations toward CD8$^+$ T cells.

Each Notch ligand induces different strengths of signaling via differential Notch receptor binding profiles.[34,38–41] To test if the CD8-biasing effect of Notch was DLL4 specific, we cultured cells on different Notch ligands during iPSC-DP-to-SP induction. We found increasing CD8 lineage bias for DLL4 > DLL1 > JAG1 ≈ JAG2, correlating with the known potency of Notch1-mediated gene activation by each ligand[34] (Figure 1G). Addition of DAPT restored CD4 lineage bias on all Notch ligands (Figure 1G). In terms of cell yields, Notch ligand choice more significantly affected 4SPs whereas DAPT more significantly affected 8SPs (Figure 1G, lower).

Overall, removing Notch signaling under optimized TCR stimulation conditions resulted in a large population of CD4$^+$ T cells that was negative for both CD8α and CD8β and expressed several mature thymocyte/naive T cell markers including CD27, CD45RA, and CD62L (Figure 1H). Pre-induction DP cells did not express CD27, expressed low CD45RA, and unexpectedly expressed high CD62L (Figure 1H). After stimulation, CD27 and CD45RA levels increased while CD62L was downregulated (Figure S1D). Maturation was similar for cells grown on different Notch ligands but with a notably lower CD27 induction on DLL4 (Figure S1D). Fluorescence-activated cell sorting (FACS) validated that both 4SP and 8SP cells could emerge directly from DPs and independently of other populations (Figure S1E).

We next assessed Notch signaling by different ligands in more detail. Analysis of iPSC-DP cells with single-cell RNA sequencing (scRNA-seq) identified low *NOTCH2* and high *NOTCH1* and *NOTCH3* expression (Figures S1F and S1G), the latter of which is targeted by JAG ligands.[41] RT-qPCR of Notch target genes (*DTX1*, *HES1*, *HES4*, *HEY1*, *NOTCH1*, and *NOTCH3*) in cells collected 3 days after SP induction on different Notch ligands indicated relative potencies DLL4 > DLL1 > JAG2 > JAG1 (Figure S1H), corresponding with known Notch1-mediated potencies[34] but leaving open the possibility that Notch2 or Notch3 play a role.

Interestingly, we observed that CD8β was downregulated much faster than CD8α during iPSC-4SP commitment (Figure S1I). This contrasts with studies of mouse thymocytes showing nearly identical kinetics for CD8α and CD8β during positive selection.[42,43] Comparing TCR$^+$CD27$^+$ cells 7 vs. 14 days after stimulation, the yield of CD4$^+$CD8β$^-$ 4SP cells at day 7 correlated well with the yield of CD4$^+$CD8β$^-$ and CD8α$^-$ 4SP cells at day 14 ($R^2$ = 0.564 and 0.57, respectively). Thus, early committed iPSC-CD4$^+$ T cells can be identified as CD3$^+$TCRαβ$^+$CD27$^+$ CD4$^+$CD8β$^-$ 4SPs even before CD8α downregulation.

We next tested if the PSC-CD4$^+$ T cell induction conditions generalize to different media conditions and cell sources. First, we applied our optimized Notch and TCR stimulation regimes to iPSC-DP cells grown in different serum-free media (Figures S2A and S2B). In all cases where TCRαβ$^+$ cells were generated, there was consistent induction of the CD4 lineage (Figures S2C and S2D). We then tested the H1 human embryonic stem cell line, and although production of DPs from H1 cells was less efficient than from our standard iPS11 line, we confirmed subsequent induction to CD4$^+$ T cells in our optimized conditions (Figure S2E).

Finally, because the anti-CD2/3/28 reagent used to induce SP differentiation engages the CD2 and CD28 co-receptors in addition to CD3, an important question is how these receptors influence SP lineage induction. First, we confirmed that both CD2 and CD28 are expressed in iPSC-DP T cells, and both are downregulated following stimulation with anti-CD2/3/28 (Figures S2F and S2G), potentially due to ligand-triggered endocytosis. We then compared SP induction by anti-CD2/3/28, anti-CD3/28, and soluble and coated anti-CD3 (clone OKT3), finding that all could generate both 4SPs and 8SPs, with the ratio dependent on dose (Figure S2H). Notably,

CellPress
OPEN ACCESS

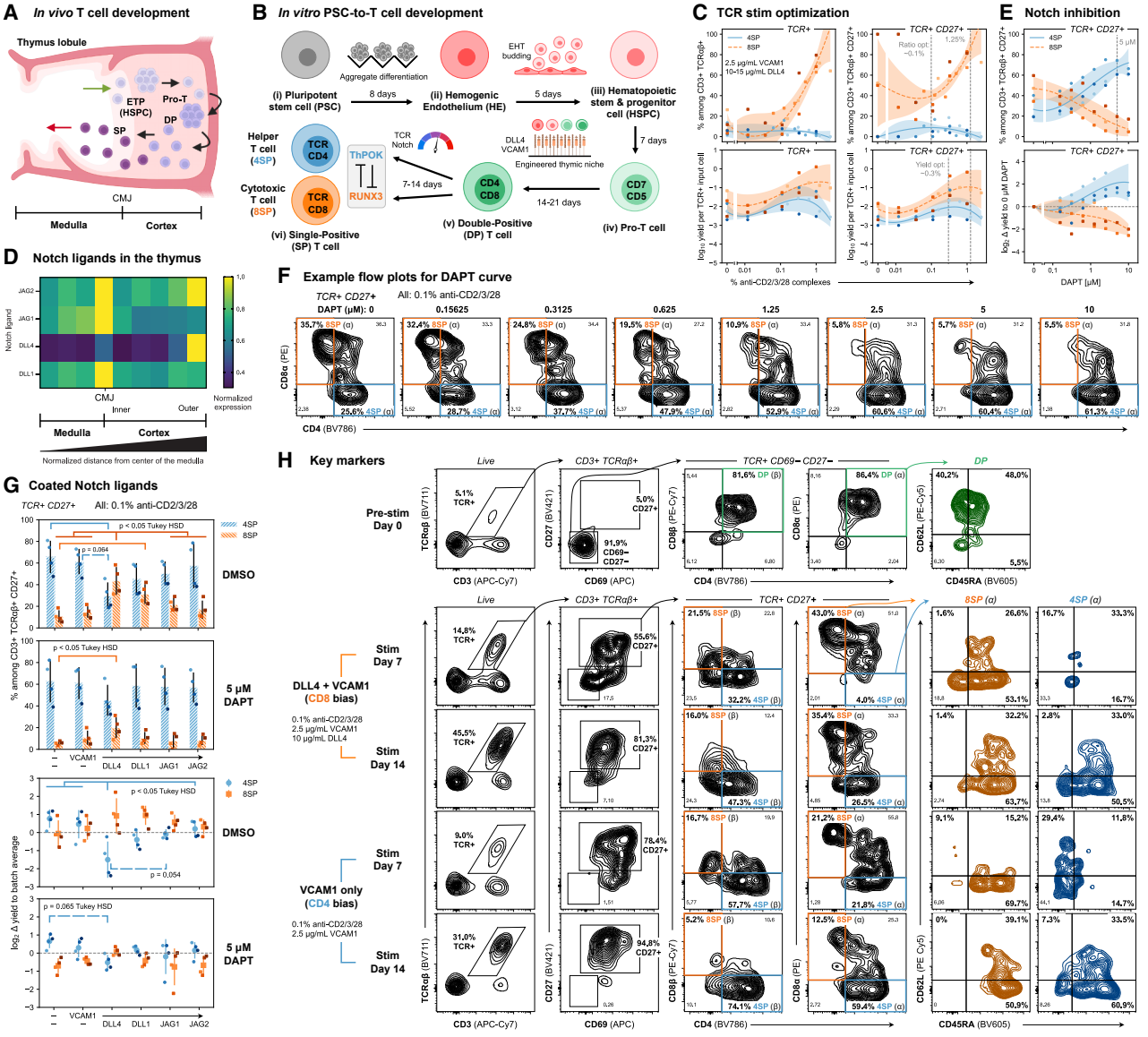


**Figure 1. Notch signaling suppresses production of CD4⁺ T cells from PSCs**

(A) Progression of human thymic T cell development. ETP, early thymic progenitor cells; HSPC, hematopoietic stem and progenitor cells; DP, $CD4^+CD8^+$ double-positive cells; and SP, CD4 or CD8 single-positive cells.

(B) Overview of *in vitro* PSC-to-T cell platform. ThPOK and RUNX3 are driving transcription factors (TFs) for $CD4^+$ and $CD8^+$ T cells, respectively.

(C) Effect of anti-CD2/3/28 levels on SP induction (day S7). Top panels: % 4SP and 8SP; bottom panels: yields per $CD3^+TCR\alpha\beta^+$ input cells pre-SP induction; left panels: $CD3^+TCR\alpha\beta^+$ ($TCR^+$) cells; right panels: $TCR^+CD27^+$ cells; 4SP: $CD4^+CD8\beta^-$; 8SP: $CD4^-CD8\alpha^+$; orange/blue lines and shaded areas: mean ± standard deviation of B-spline smoothed measurements for each differentiation ($n = 4$); gray dashed lines indicate the standard concentration of anti-CD2/3/28 (1.25%) and optima for the percent (~0.1%) or yield (~0.3%) of 4SPs.

(D) Relative expression of different Notch ligands in human post-natal thymus, averaged across lines drawn from the center of the medulla to edge of the cortex in $n = 3$ thymus lobules.

(E) Effect of Notch signaling inhibition by the γ-secretase inhibitor DAPT on SP induction (0.1% anti-CD2/3/28, day S14). Lines + shaded areas are derived from B-splines as in (C); $n = 3$ differentiations.

(F) Representative flow plots for cells in (E) for each level of DAPT tested.

(G) Effect of Notch ligands ± DAPT on SP induction (0.1% anti-CD2/3/28, day S14). Values are mean ± standard deviation; $n = 4$ differentiations; statistical significance was determined by one-way ANOVA with HSD post hoc test and a significance threshold of $p > 0.05$; detailed statistics are provided in Table S1.

(H) Representative flow plots for cells in (G) before and after SP induction ± DLL4 (both −DAPT).

See also Figures S1 and S2.

co-receptor co-stimulation gave higher cell yields than CD3 stimulation alone, although yields sharply decreased at high levels of both the coated anti-CD3 and co-receptor-targeting reagents, suggesting negative selection.

## Tuning Notch and TCR stimulation controls the ratio of iPSC-CD4$^+$ vs. CD8$^+$ T cells

The ratio of CD4 to CD8 T cells is an important factor in the efficacy of CAR-T cell therapy,[18,44] so we next tested whether we could control this ratio in a single culture during iPSC-SP induction by modulating levels of both Notch and TCR stimulation (Figure 2A). In addition, we hypothesized that different TCR pathway stimulation methods might influence CD4 vs. CD8 lineage bias. We therefore compared anti-CD2/3/28 to phytohemagglutinin (PHA) and phorbol myristate acetate (PMA) plus ionomycin (Iono) (Figure 2A). PHA is a lectin that non-specifically cross-links glycosylated cell surface proteins, including the TCR; whereas PMA is an analog of diacyl glycerol (a TCR signaling intermediate), often used with Iono, a calcium ionophore, to recapitulate TCR signaling independently from direct TCR stimulation.

As with anti-CD2/3/28, there were optimal doses of PHA and PMA+Iono for induction of 4SP cells. Decreasing DLL4 increased the percent and yield of 4SP cells in all cases, while also decreasing 8SP yields at high anti-CD2/3/28 or PHA levels (Figures 2B and S3A). In the absence of stimulating inputs, there was a strong bias in spontaneous differentiation toward 8SP cells, likely due to infrequent MHC class II$^+$ cells.[33] Notably, the proportion of TCR$\alpha\beta^+$ cells that acquired a mature phenotype (CD45RA$^+$CD62L$^+$) also increased with decreasing DLL4 (Figures 2B and S3B), corresponding with our prior observations with CD27 (Figure S1C). For PHA, the overall phenotype pattern was similar to anti-CD2/3/28, with both reagents generating mature CD4$^+$ T cells. Interestingly, the optimal dose of PMA for CD4$^+$ T cell induction (0.25 ng/mL) gave the lowest percent of CD45RA$^+$CD62L$^+$ cells, suggesting reduced maturation. After PMA+Iono stimulation, cells strongly decreased expression of CD45RA and CD62L while only weakly upregulating CD27 from an initial CD27$^-$CD45RA$^{lo}$CD62L$^+$ phenotype (Figure S3C). To test if lack of co-stimulation limited maturation of PMA+Iono-stimulated cells, we added 1 μg/mL soluble anti-CD28 but saw similar results to PMA+Iono alone (Figure S3C).

Overall, our various conditions enabled production of broad 4SP:8SP ratios (Figure 2C). PMA+Iono stimulation resulted in the highest proportion of 4SPs but with lower yields (Figures 2D, 2E, and S3A). Notably, there were many conditions with high yields of both 4SPs and 8SPs (Figure 2D). Conditions that generated intermediate 4SP:8SP ratios showed the highest variance across replicates (Figure 2F). This variation was highest with anti-CD2/3/28 and lowest with PMA, possibly indicating differential sensitivity to factors such as cell density and population composition. Overall, these results indicate that modulating Notch and TCR stimulation is a broadly applicable strategy to tune CD4$^+$ vs. CD8$^+$ T cell production from PSCs.

## iPSC-CD4$^+$ T cells are mature and expandable *in vitro*

To further evaluate our PSC-CD4$^+$ T cell induction protocol, we investigated expression of naive T cell markers and lineage-defining TFs ThPOK (CD4) and RUNX3 (CD8). iPSC-DP cells were cultured in conditions optimized to remain DP or differentiate to 4SP or 8SP, using either anti-CD2/3/28 or PHA (Figure 3A), and 1 week later, the expected cell-type bias was confirmed (Figure 3B). As expected, 4SPs strongly upregulated ThPOK relative to DPs and 8SPs. Interestingly, 4SPs also expressed RUNX3, albeit at a lower level than 8SPs (Figure 3C), like in mature 4SP thymocytes.[43,45] Compared with DPs , newly committed 4SPs and 8SPs significantly upregulated CCR7 (Figure S4A). Expression of these markers was nearly identical between anti-CD2/3/28 and PHA stimulation. Focusing on 4SPs, we observed significant upregulation of CD27 upon commitment from DPs with heterogeneous CD62L expression (Figure 3D). Newly committed 4SPs preferentially expressed the CD45RO isoform but gradually switched to CD45RA after an additional week of rest (Figure 3E).

Next, we investigated if sorted iPSC-CD4$^+$ T cells (Figure S4B) could be expanded while retaining their 4SP phenotype. Over the course of 14 days, with restimulation at day 7, the cells proliferated ~15-fold while retaining the 4SP phenotype in >80% of cells (Figure 3F). As expected, amounts of interleukin (IL)-2 dictated the extent of proliferation but did not induce proliferation without TCR stimulation (Figure S4E).

Finally, we assessed if stimulation of iPSC-CD4$^+$ T cells with anti-CD2/3/28 upregulated relevant markers of activation and co-stimulatory function. As a comparator, CD4$^+$ T cells isolated from post-natal thymus or adult peripheral blood were tested in parallel (Figures S4C and S4D). Relative to unstimulated conditions, iPSC-CD4$^+$ T cells significantly upregulated all markers tested (CD71, 4-1BB, OX40, and CD40L) to levels closer to thymic than adult blood CD4$^+$ T cells (Figures 3G and S4F). Overall, like primary T cells, iPSC-CD4$^+$ T cells expanded and proliferated *in vitro*, retained their CD4 phenotype, and upregulated relevant markers of activation and co-stimulation.

## Notch suppresses TCR signaling and ThPOK to bias toward CD8$^+$ T cells

To better understand the mechanism by which Notch and TCR input signals control CD4 vs. CD8 lineage commitment in PSC-T cells, we induced iPSC-derived DPs to SPs and measured key TCR signaling pathway member phosphorylation and lineage TF expression using intracellular flow cytometry. We tested six conditions with different lineage biases: either low anti-CD2/3/28 (0.3%, CD4-biased) or high anti-CD2/3/28 (1.25%, CD8-biased); each −DLL4/−DAPT (CD4-biased), +DLL4/−DAPT (CD8-biased), or +DLL4/+DAPT (CD4-biased) (Figures 4A, 4B, and S5A).

Following stimulation in all conditions, TCR expression sharply decreased over the first 1–3 days before rebounding (Figure 4B, top left). Among iPSC-derived CD3$^+$TCR$\alpha\beta^+$ cells, different ratios of CD4$^+$CD8$\alpha^-$ 4SPs or CD4$^-$CD8$\alpha^+$ 8SPs emerged as expected per condition (Figure 4B, top right). Along with suppressing 4SP induction, +DLL4/−DAPT conditions retained more DPs and reduced TCR reactivation. As before (Figure S1I), we saw faster downregulation of CD8β than CD8α in 4SP-committing cells (Figure S5B). Strikingly, committed CD27$^+$CD4$^+$CD8$\beta^-$ 4SPs appeared within 1 day of stimulation and were remarkably stable throughout the time course for conditions −DLL4/+DAPT (Figure S5B, bottom right). This is consistent with the notion that CD27 marks stably committed cells[36] and with recent work indicating CD4 lineage commitment is much more rapid than CD8.[50] Finally, CD27 induction was reduced by ~20–30

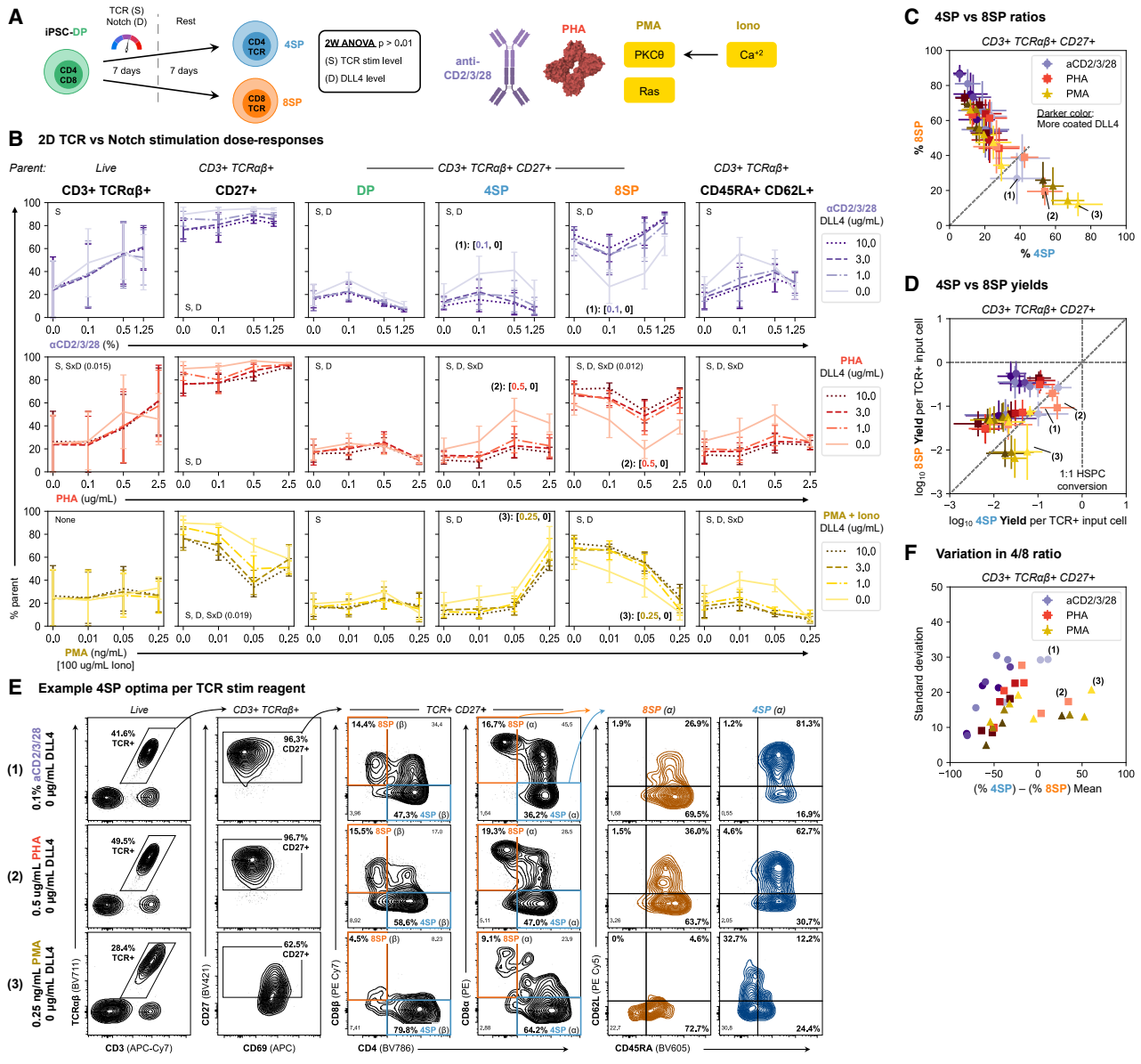


**Figure 2. Tuning Notch and TCR stimulation controls the ratio of iPSC-CD4$^+$ vs. CD8$^+$ T cells**

(A) Overview of experiment design and TCR stimulation modalities (anti-CD2/3/28, PHA-M, PMA + Iono).

(B) Effects of Notch and TCR stimulation on SP induction and maturation. The labels (1), (2), and (3) across (B)–(F) highlight conditions that optimize the ratio of 4SP to 8SP cells. 4SP: CD4$^+$CD8β$^-$; 8SP: CD4$^-$CD8α$^+$; values are mean ± standard deviation; $n$ = 4 differentiations; inset indicators D and S refer to significance of DLL4 levels (D), TCR stim input levels (S), and interactions (x) with each other, using two-way ANOVA with a significance threshold of $p < 0.01$; $p$ values close to but above the significance threshold are shown; detailed statistics are provided in Table S1.

(C and D) Comparison of the percent (C) and yield per CD3$^+$TCRαβ$^+$ input (D) of TCR$^+$CD27$^+$ 4SP vs. 8SP cells across all conditions with non-zero TCR stimulation input levels. Darker colors indicate increasing concentrations of coated DLL4.

(E) Representative flow plots for optimal 4SP-inducing conditions (1), (2), and (3) for each TCR-stimulating reagent.

(F) Comparison of the mean and standard deviation in the percent of cells that commit to CD4$^+$ vs. CD8$^+$ T cells across all conditions. Coloring as in (C) and (D). See also Figure S3.

percentage points in conditions +DLL4/−DAPT 7–14 days post-stimulation (Figure 4B, bottom left), consistent with our prior observations (Figures S1C, 2B, and S3C).

Like CD27, the TCR stimulation marker CD69 was reduced in -+DLL4/−DAPT conditions (Figure 4C). Conditions with high anti-CD2/3/28 input (1.25%) induced higher CD69 expression but slowed the post-stimulation recovery of TCR expression (Figure 4C, right). This may result from higher stimulation input triggering more TCR ubiquitination and downregulation.[51,52]

We next examined phosphorylation of key TCR signaling pathway members during a 72 h window following stimulation. Overall, we observed pulse-like stimulation responses for

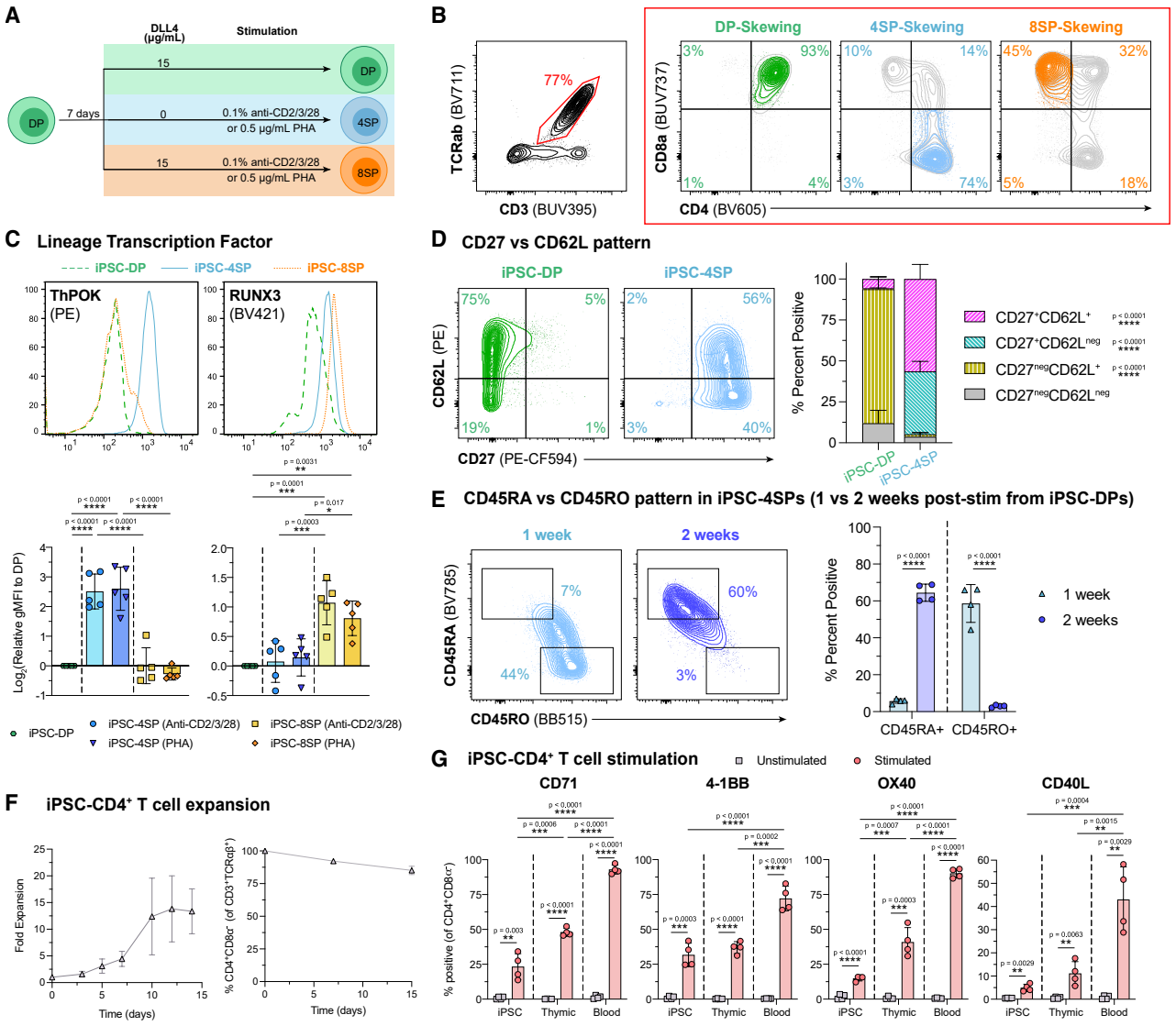


**Figure 3. iPSC-CD4⁺ T cells are mature and expandable *in vitro***

(A) Overview of experiment design and SP-skewing conditions.

(B) Representative flow plots of CD4 vs. CD8α expression pattern in CD3⁺TCRαβ⁺ cells (day S7).

(C) Top: representative histograms of ThPOK and RUNX3 expression in iPSC-DPs, -4SPs, and -8SPs; Bottom: $\log_2$-transform of each marker's relative geometric mean fluorescence intensity (gMFI) of iPSC-4SP/-8SP normalized to iPSC-DPs. Day S7; values are mean ± standard deviation; $n = 5$ differentiations; statistical significance was determined using ordinary one-way ANOVA followed by Tukey HSD test, with $p$ values shown.

(D) Representative flow plots comparing CD27 vs. CD62L expression pattern in iPSC-DPs and iPSC-4SPs (PHA-L-derived), and each subset is quantified in stacked bar charts on the right. Day S7; values are mean ± standard deviation; $n = 4$ differentiations; statistical significance was determined using unpaired $t$ test with $p$ values shown.

(E) Representative flow plots comparing CD45RA vs. CD45RO expression pattern in iPSC-4SPs (PHA-L-derived), 1 week vs. 2 weeks post-stimulation in 4SP-skewing condition in (A). Percent CD45RA⁺ and CD45RO⁺ quantified in bar chart on the right. Values are mean ± standard deviation; $n = 4$ differentiations; statistical significance was determined using unpaired $t$ test with $p$ values shown.

(F) Left: fold expansion of sorted iPSC-4SPs; right: percent 4SP cells (CD4⁺CD8α⁻ within CD3⁺TCRαβ⁺) throughout expansion. Values are mean ± standard deviation; $n = 3$–5 differentiations.

(G) T cell activation markers following 48 h TCR stimulation for expanded iPSC-CD4⁺ T cells vs. primary thymic and blood 4SP counterparts. Values are mean ± standard deviation; $n = 4$ differentiations or $n = 4$ thymic donors or blood donors. Statistical significance was determined using unpaired $t$ test (between unstimulated and stimulated cells in each of iPSC-, thymic-, and blood-derived cells) and ordinary one-way ANOVA followed by Tukey HSD test (for stimulated cells between iPSC-, thymic-, and blood-derived cells), with $p$ values shown. Detailed statistics are provided in Table S1.

See also Figure S4.

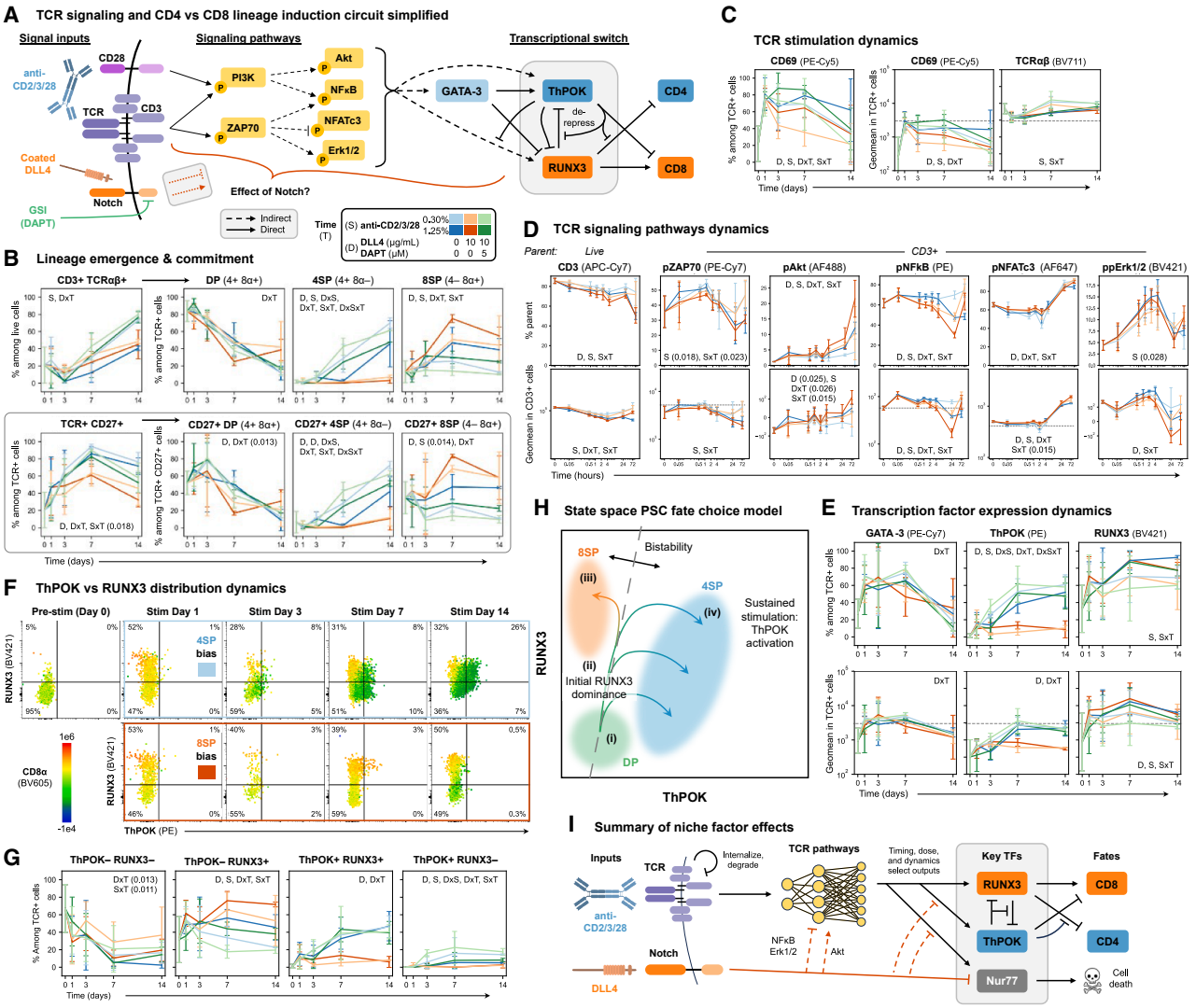


**Figure 4. Notch suppresses TCR signaling to bias toward CD8⁺ T cells**

(A) Simplified CD4 vs. CD8 lineage induction circuit.[28,46,47–49] Solid vs. dashed lines indicate direct vs. indirect interactions, respectively. This experiment aimed to uncover the effects of Notch and TCR stimulation on this circuit.

(B–E) Dynamics of (B) TCR, CD27, CD4, and CD8α surface expression; (C) CD69 and TCRαβ surface expression; (D) phosphorylation of key TCR/CD28 signaling pathway members; and (E) TF expression. Inset indicators D, S, and T refer to significance of DLL4/DAPT variants (D), anti-CD2/3/28 levels (S), and interactions (x) with each other and time (T) using three-way ANOVA with a significance threshold of $p < 0.01$; $p$ values close to but above the significance threshold are shown; detailed statistics are provided in Table S1.

(F and G) RUNX3 vs. ThPOK expression overlayed with CD8α expression in key CD4- vs. CD8-biased conditions (F) and compared across conditions (G).

(H) Model of cell progression through ThPOK vs. RUNX3 state space during iPSC-DP-to-SP induction.

(I) Summary of how anti-CD2/3/28 and Notch inputs affect downstream gene expression to bias CD4 vs. CD8 lineage commitment.

For (B), (C), (E), and (G): values are mean ± standard deviation; $n = 4$ differentiations ($n = 2$ at day S14). For (D): values are mean ± standard deviation; $n = 3$ independent differentiations. Dashed lines in geomean plots indicate positive gate thresholds.

See also Figure S5.

pZAP70 and ppErk1/2 and to a lesser degree pNF-κB and pNFATc3 (Figure 4D), likely caused by a combination of TCR downregulation, induction of negative feedback regulators like dual specificity phosphatases,[53] and upregulation of suppressive receptors like CD5[54] (Figures S2F and S2G). pAkt gradually increased over time, with strong increases between 24 and 72 h in some conditions.

At the higher concentration (1.25%), anti-CD2/3/28 induced greater reductions in pZAP70, pNF-κB, and ppErk1/2 levels between 24 and 72 h, consistent with the enhanced TCR downregulation noted above, suggesting engagement of stronger negative feedback mechanisms. Notch signaling also drove similar reductions for pNF-κB and ppErk1/2 and a slight increase in pNFATc3. The combined result was more constant pNF-κB

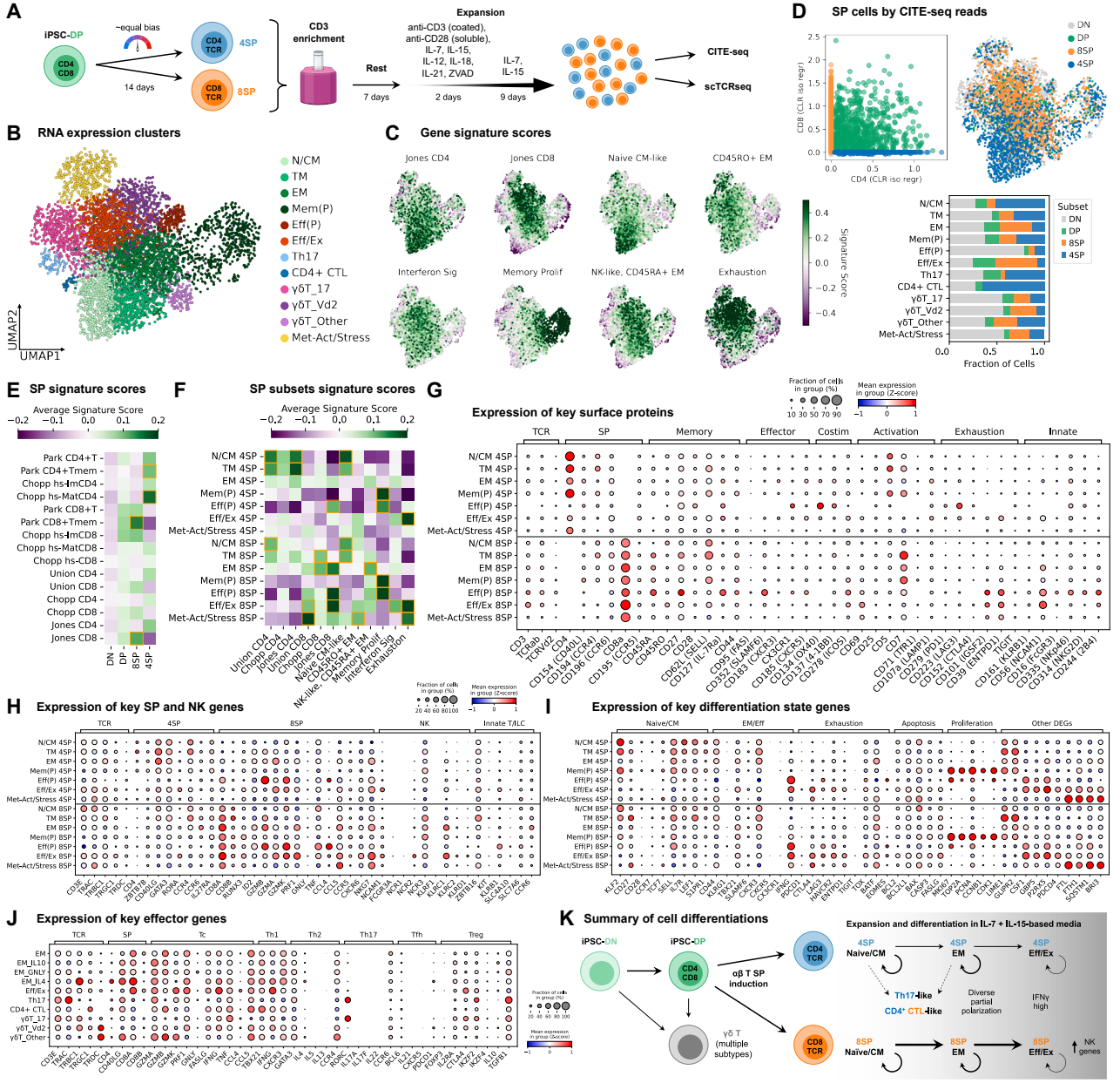


**Figure 5. iPSC-CD4$^+$ and -CD8$^+$ T cells express expected lineage genes**

(A) Production and expansion of iPSC-derived T cells for CITE-seq + scTCR-seq.

(B) Uniform manifold approximation and projection (UMAP) and RNA Leiden[65]-based clusters identified a gradient of iPSC-T cell states that resembled T cell differentiation states (N, naive; CM, central memory; TM, transitional memory; EM, effector memory; P, proliferating; and Eff/Ex, effector/exhausted), as well as Th17-like cells, CD4$^+$ cytotoxic T lymphocyte (CTL)-like cells, and three types of γδ T cells.

(C) UMAPs with key gene signature scores overlayed (functional signatures from Mazziotta et al.[66]). Signature scores for each cell are the average *Z* score of signature gene expression levels relative to that of a set of background genes. All signature genes are listed in Table S2.

(D) Left: "gating" 4SP and 8SP cells via CITE-seq reads (normalized via centered log ratio [CLR] and isotype regression[67]). Right: the distribution of gated populations throughout the UMAP space. Bottom: distribution of SP gated populations within each cluster. Gate thresholds were determined by a 3-component Gaussian mixture model (GMM) using ThresholdPy (adapted here from ThresholdR[68] to Python).

(E) Scoring of gated cells for CD4$^+$ and CD8$^+$ T cell signature genes.[43,69] The heatmap shows averaged scores for cells in each gated population; orange boxes: score > 0.1; contributions from individual genes are provided in Table S3.

(F) Scoring of 4SP and 8SP gated cell subsets per differentiation state-based cluster for main CD4 and CD8 signature genes and functional signature genes.[66] Orange boxes: score > 0.1; contributions from individual genes are provided in Table S4.

(G) Expression of key surface proteins captured with CITE-seq in different 4SP/8SP populations. A two-component GMM was used via ThresholdPy to find thresholds and set all values below them to 0 (more restrictive than the SP gating thresholds); scaled values (*Z* scored across cells) were used for visualization.

*(legend continued on next page)*

and ppErk1/2 levels in the 4SP-optimal conditions (−DLL4, 0.3% anti-CD2/3/28). Interestingly, the pattern was reversed for pAkt, raising the possibility that Akt-mTOR signaling plays a role in 8SP induction *in vitro*. Akt phosphorylation may have been driven by indirect or non-canonical Notch signaling[55] and/or IL-7 signaling,[56] a key driver of 8SP commitment.[57] Indeed, the fraction of cells expressing IL7Rα (CD127) increased the most after TCR stimulation in +DLL4/−DAPT conditions (Figure S5C).

In all conditions, expression of GATA-3, a key CD4 lineage-driving TF,[58,59] rapidly increased within 1 day of stimulation, then slowly decreased between days 3 and 14 (Figure 4E, left). The decrease was faster in +DLL4/−DAPT conditions, potentially due to reduced TCR pathway activation.[60] Conversely, ThPOK expression was almost completely blocked in Notch-stimulating conditions (Figure 4E, middle), directly linking to the CD8 lineage bias of Notch. Unexpectedly, we observed rapid and strong induction of RUNX3 in all conditions, with higher levels in conditions with higher (1.25%) anti-CD2/3/28 input (Figure 4E, right). This contrasts with *in vivo* DP-to-SP transitions, where RUNX3 activation is delayed.[28]

Examining the joint expression distribution of ThPOK and RUNX3, we saw that most ThPOK$^+$ cells also expressed RUNX3 (Figures 4F and 4G), aligning with our previous end-stage measurements (Figure 3C). ThPOK and CD4 expression were directly correlated, whereas many RUNX3$^+$ cells were CD8α$^-$ and expressed high levels of ThPOK (Figures S5D and S5E), consistent with ThPOK's ability to self-activate, prevent RUNX3 silencing of *ThPOK* and *CD4* genes, and to suppress the *CD8* locus.[46] The level of CD8α corresponded with the ratio of ThPOK vs. RUNX3, consistent with the TFs competing to repress and activate the *CD8* locus, respectively.[61,62] The gradual increase in ThPOK levels over time (Figures 4E and 4G), compared with the more rapid CD4 lineage commitment inferred by CD4 vs. CD8β expression in TCR$^+$CD27$^+$ cells (Figure S5B), aligns with ThPOK's reported role in "sealing" rather than initiating CD4 fate.[43]

To explain our TF observations, we put forward a state space model of PSC-derived T cell commitment (Figure 4H). RUNX3 is initially upregulated by stimulated PSC-DPs, and differences in TCR and Notch input levels result in either RUNX3 or ThPOK dominance, respectively leading to CD8 or CD4 lineage bias (Figure 4H). At a critical boundary ratio of ThPOK vs. RUNX3 levels, the system is bistable and cells can stochastically commit to either lineage, leading to higher variability in the percent of 4SP vs. 8SP cells in equal-bias conditions (Figure 2F).

Overall, high levels of anti-CD2/3/28 downregulate TCR expression and increase negative feedback and RUNX3 expression, contributing to CD8 lineage bias (Figure 4I). Strong Notch signaling by DLL4 reduces TCR-driven NF-κB and Erk1/2 signaling and downstream outputs—especially ThPOK—thereby suppressing the CD4 lineage (Figure 4I). Notch also increases TCR-driven Akt signaling and suppresses induction of the pro-apoptotic negative selection gene *NR4A1* (Nur77, as seen in our qPCR data: Figure S1H), and it may directly inhibit Nur77 itself,[63] thereby promoting cell survival and reducing negative selection.

## iPSC-CD4$^+$ and -CD8$^+$ T cells express expected lineage genes

To further characterize iPSC-CD4$^+$ T cells, we performed CITE-seq (cellular indexing of transcriptomes and epitopes by sequencing) and scTCR-seq (single-cell TCR sequencing) on iPSC-T cells. The cells were differentiated to an approximately equal ratio of 4SP and 8SP cells, magnetically enriched for CD3$^+$ cells, then expanded for 11 days in IL-7/IL-15-based media[13,64] prior to sequencing (Figure 5A). Clustering identified a combination of αβ and γδ T cells, with the αβ T cells taking on diverse states resembling naive (N), central memory (CM), transitional memory (TM), effector memory (EM), and effector/exhausted cells, including small clusters of CD4$^+$ T cells in Th17- and cytotoxic-like states (Figure 5B). Clusters were labeled based on signature gene expression scores, differentially expressed genes, and manual assessment of protein and RNA expression patterns (Figures 5C and S6A–S6C; Table S3).

After normalizing CITE-seq protein measurements to account for non-specific binding and remove background (Figures S6D and S6E; see STAR Methods), we gated cells for surface expression of CD4 vs. CD8 (Figure 5D). 4SPs were predominantly found in naive and memory states while 8SPs were mostly EM and effector/exhausted (Figure 5D). This distribution was likely influenced by our specific expansion conditions and was not necessarily inherent to the cells. Evaluation with previously described[43,69] and newly defined (Union/Jones CD4/CD8, see STAR Methods) signature gene sets confirmed that gated 4SPs and 8SPs matched the respective expected signatures of CD4$^+$ and CD8$^+$ mature thymocytes or T cells (Figure 5E; Table S4). A subset of cells expressed CD4 and CD8 (DP) and showed modest scores for both gene sets, suggesting they reflect anomalous CD4 or CD8 re-expression in expanded 8SPs or 4SPs, consistent with our earlier observations in Figure 3F, rather than representing residual immature DP T cells.

We next evaluated 4SPs and 8SPs within each main differentiation state cluster (N/CM, TM, EM, Mem(P), Eff(P), Eff/Ex, and Met-Act/Stress). While N/CM and TM subsets generally showed higher CD4 signature scores, and Eff/Ex subsets generally showed higher CD8 signature scores (Figure 5F; Table S5), CD4 and CD8 signature scores were stronger in the respective SP gated cells across all clusters except Eff(P) (Figure S6F). Other notable differences included stronger NK-like/CD45RA$^+$ EM and interferon signaling scores for 8SP Eff/Ex cells than for their 4SP counterparts, suggesting the former may have innate features, as often seen in iPSC-derived 8SPs.[14,70] Indeed, analysis of surface protein expression in each cluster (Figures 5G and S6G) showed notable levels of CD56, NKp46 (CD335), NKG2D (CD314), and 2B4 (CD244) in some 8SP Eff/Ex cells. Other

(H–J) Expression of key genes in different 4SP/8SP populations and clusters, including EM subclusters in (J). Scaled values (*Z* scored across cells) were used for visualization.
(K) Summary of sequencing results, highlighting the emergence of diverse cell types and divergent differentiation rate of 4SPs vs. 8SPs.
See also Figure S6.

surface markers generally followed expected patterns, with notable differences in costimulatory and exhaustion markers; 4SP Eff/Ex cells expressed more OX40, 4-1BB, PD1, and LAG3, while 8SP Eff/Ex expressed more ICOS, CD101 (*IGSF2*), and CD39 (*ENTPD1*) (Figure 5G).

Examining transcript patterns (Figures 5H and S6H) confirmed differential expression of broad CD4 and CD8 lineage genes across the clustered/gated subsets, as well as the generally higher expression of NK genes in the 8SP clusters. As expected, granzymes (*GZMB*, *GZMA*) and perforin (*PRF1*) were lower in 4SP clusters vs. 8SP counterparts, suggesting reduced cytotoxicity. Unexpectedly, CCR6, a marker of memory CD4$^+$ T cells and Th17 cells, was higher in most 8SP subsets compared with their 4SP counterparts, potentially reflecting a CD8$^+$ NKT-like phenotype in the latter.[71] Indeed, the innate T cell TF PLZF (*ZBTB16*, key for NKTs) was expressed most highly in TM 8SPs. Other innate T cell- and ILC-specific genes were expressed weakly or only in certain subsets.

Focusing on memory/differentiation-associated genes (Figures 5I and S6H), we confirmed that N/CM/TM 8SPs and 4SPs expressed expected genes including *KLF2*, *CD27*, *SELL* (CD62L), *IL7R*, *LEF1*, and *S1PR1*. Likewise, more differentiated cells upregulated expected genes including *TBX21* (T-BET) and *IFNG*. Apoptosis markers were generally higher in Eff/Ex subsets, compared with less differentiated cells, although N/CM subsets showed a notably high expression of the pro-apoptotic protein *BAX*. Other notable differentially expressed genes across differentiation states (for both 4SPs and 8SPs) included *LIME1* (TCR interactor) and *GLIPR2* (positive regulator of Erk1/2) in N/CM/TM/EM/Mem(P) subsets, followed by *CSF1*, *GBP5* (IFN-induced), *P2RX5*, and *PDCD4* in Eff(P)/Eff/Ex subsets. This pattern reflects a transition toward more activated,[72,73] inflammatory signaling states with potentially decreased TCR signaling responsiveness. Expression of iron storage genes (*FTL*, *FTH1*) and stress-responsive genes (*SQSTM1*, *BRI3*) indicated a cluster of cells containing both 4SPs and 8SPs was metabolically active and stressed.

Finally, we examined the emergence of different effector states (Figure 5J). A cluster of αβ T cells was Th17-like, although these cells did not have detectable expression of IL-17 and expressed surprisingly high *TGFB*. A γδ T cell cluster showed a similar pattern and was annotated γδ17 cells. Two other γδ T cell subsets (one Vd2-expressing) were present, and both had a cytotoxic/Th1-like profile. Within the EM population, there were notable subclusters with divergent expression of key effector genes, including *IL4*, *IL10*, *TGFB*, *IFNG*, and granulysin (*GLYN*), but with no clear pattern matching a particular Th or cytotoxic subset. These likely represent mixed populations of cells with emerging divergent functions. *FOXP3* mRNA was nearly absent across all subsets, indicating little to no Treg differentiation.

Overall (Figure 5K), iPSC-CD4$^+$ and -CD8$^+$ T cells take on unique transcriptional profiles that largely correspond with expected human memory and effector T cell transcriptomes. The iPSC-4SPs largely retained a naive/memory-like state while the iPSC-8SPs acquired more effector and innate-like features. The cells began to adopt diverse effector states, indicating their potential for greater functional divergence under polarizing conditions.

## iPSC-CD4$^+$ T cells express a diverse TCR repertoire

Producing T cells from PSCs *in vitro* is valuable for modeling and recreating T cell development and TCR repertoire formation.[74] We thus leveraged our platform to study TCR repertoires in iPSC-CD4$^+$ vs. CD8$^+$ T cells. As *in vivo*-differentiated references, we used human thymocyte-[69] and peripheral blood mononuclear cell (PBMC)-derived T cells.[75] The iPSC-derived DP, 4SP, and 8SP CITE-seq-gated populations expressed diverse TCR sequences, although less diverse than *ex vivo* thymocytes and PBMC T cells (Figure 6A). This may be due to the iPSC-T cell expansion step prior to sequencing (Figure 5A), which can promote oligoclonality. As with recent studies of PSC-CD8$^+$ T cells by our lab and others,[13,14,33] all iPSC-derived cells expressed TCRs with short fetal thymocyte-like CDR3 lengths (Figure 6B), indicating low TdT levels during TCR rearrangement and positive selection,[76] limiting diversity.

We next analyzed TCR V(D)J rearrangement patterns that, in primary thymocytes, show stage-specific biases via genomic looping and proximity[69,78] (Figure 6C). TCRs in both iPSC-CD4$^+$ and CD8$^+$ T cells used diverse V and J segments across the entire TCRα and β loci (Figures 6D and 6E). Notably, all iPSC-T cells showed a unique pattern of Vβ chain usage for several segments near the center of the Vβ array (Figure 6D), but the overall density of Vβ chains was otherwise similarly dispersed throughout the array (Figure 6F). All iPSC-T cell types infrequently used middle Jβ segments relative to primary cell types (Figures 6D and 6F).

TCRα chain usage was similar between iPSC-T cells and all primary cell types except fetal DP thymocytes (Figure 6E). iPSC-T cell Vα patterns were highly enriched for fragments near the center of the Vα array, with the overall density resembling post-natal thymocyte- and PBMC-CD4$^+$ T cells (Figure 6F). Notably, iPSC-CD4$^+$ and DP cells differentially expressed TRAV14-01 while iPSC-CD8$^+$ cells differentially expressed TRAV21-01, both of which are enriched in primary CD8$^+$ T cells (Figure 6E). iPSC-T cell Jα patterns were enriched for fragments near the 5′ end of the Jα array, with overall densities resembling fetal thymocyte-CD4$^+$ T cells and PBMC-CD8$^+$ T cells (Figures 6E and 6F). The relatively infrequent use of distal Vα/Jα segments in iPSC-T cells could be due to an interruption of the serial α chain recombination process by artifiical TCR stimulation during SP induction.

Finally, we clustered relative V(D)J fragment usages for each cell type using principal-component analysis (PCA) (Figure 6G). Primary CD4$^+$ and CD8$^+$ T cell types clustered separately, as expected,[69] whereas the iPSC-derived T cells clustered separately from both each other and primary cell types. Overall, these data point to a unique TCR rearrangement process in iPSC-T cells with notable biases between iPSC-CD4$^+$ and CD8$^+$ T cells.

## iPSC-CD4$^+$ T cells can polarize into functionally distinct T helper subsets

A hallmark of CD4$^+$ T cells is their ability to respond to specific cytokines and polarize into specialized, helper subsets that direct and enhance the function of other immune cells.[79] To test if iPSC-CD4$^+$ T cells have this capacity, we stimulated iPSC-, post-natal thymic-, and adult blood-derived CD4$^+$ T cells with anti-CD2/3/28 in the presence or absence (Th0) of

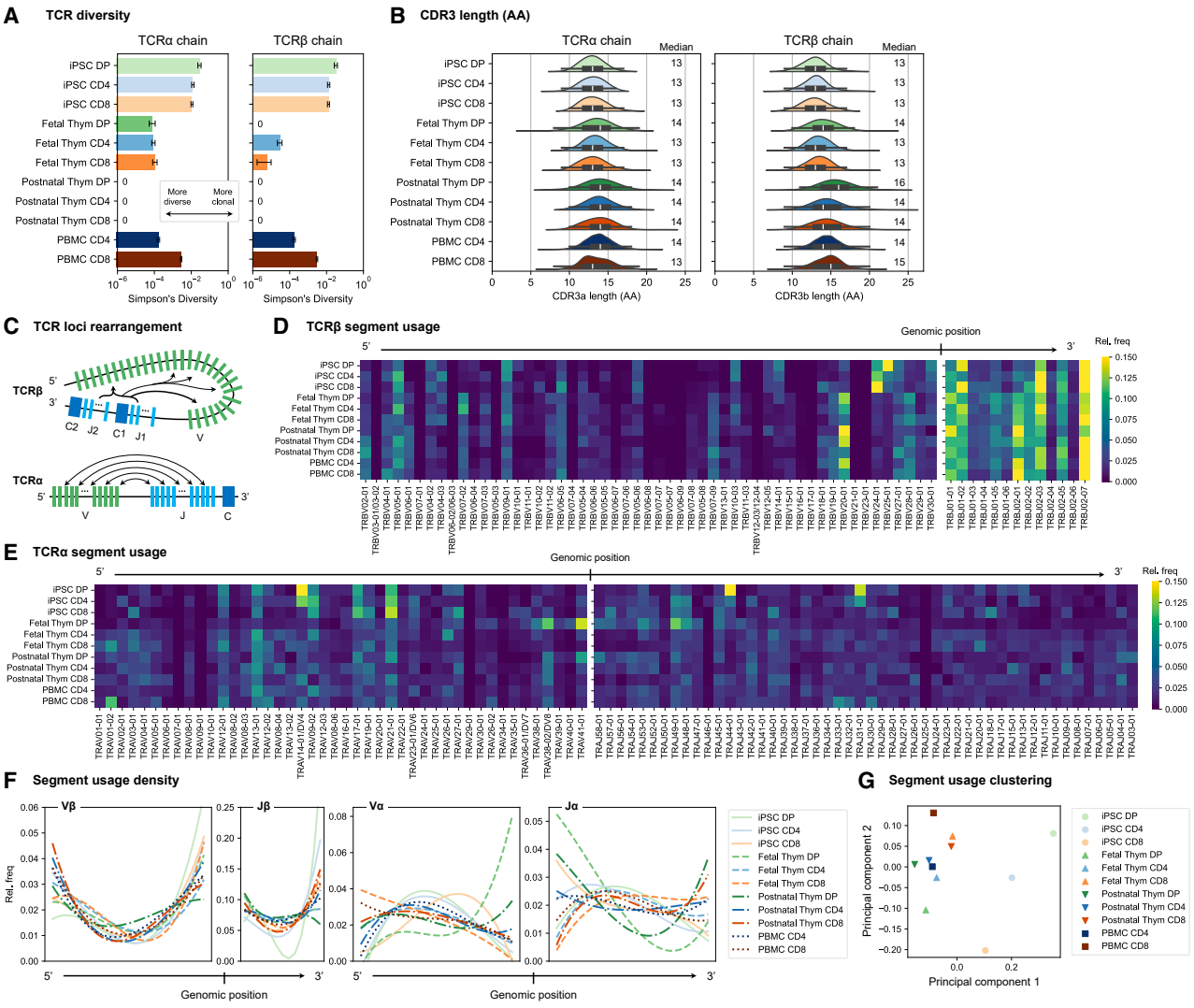


**Figure 6. iPSC-CD4⁺ T cells express a diverse TCR repertoire**

(A) Simpson's diversity for unique TCR clones (CDR3 + V + J rearrangements). Smaller numbers indicate higher diversity. Error bars: unbiased estimation of standard deviation[77]; iPSC-DP, CD4, and CD8 cells correspond to the CITE-seq-gated DP, 4SP, and 8SP cells in Figure 5D, further filtered for cells with a captured TCR sequence.

(B) Comparison of CDR3 amino acid sequence lengths.

(C) Positional bias of TCR loci rearrangement (adapted from Park et al.[69]).

(D and E) TCRβ (D) and TCRα (E) chain segment usages across iPSC-, thymic-, and blood-T cells. Segments are ordered based on genomic position; frequencies of each row sum to 1.

(F) B-spline smoothed segment usage densities for each array.

(G) PCA-based clustering of combined TCRα and TCRβ segment usage frequencies for each row in (D) and (E).

Th1-, Th2-, or Th17-polarizing cytokines[80] for 7–14 days. Cells were assessed for Th1/2/17-associated TFs, chemokine receptors (CRs), and cytokines (Figure 7A). Under Th0, Th1, and Th2 conditions, expression of CD4 and CD8α was stable across cell sources (iPSC, thymic, and blood), with a small population of DPs emerging in both iPSC- and thymic-CD4⁺ T cells. However, under Th17 conditions, a significant fraction of DN and 8SP cells emerged in iPSC-derived, but not thymic- or blood-derived, cells (Figures S7A and S7B).

Polarized cells were phenotyped by flow cytometry for Th-related TFs (T-BET for Th1, GATA-3 for Th2, RORγt for Th17) and CRs (CXCR3 for Th1, CCR4 for Th2, CCR4 and CCR6 for Th17), and expression levels were normalized to Th0 cells in the unpolarized condition (Figures 7B, 7C, S7C, and S7D). Relative to other Th subsets, iPSC-Th1 upregulated T-BET and CXCR3 expression, similarly to thymic- and blood-Th1 cells. Under Th2 conditions, iPSC-Th2 cells upregulated GATA-3 similarly to blood-Th2 cells, but unlike thymic- and blood-Th2 cells, they downregulated CCR4. Relative to Th0, iPSC-Th17 minimally upregulated RORγt but significantly upregulated CCR4 and CCR6, as did thymic- and blood-Th17 cells. T-BET was expressed in all iPSC-Th subsets except Th17 but

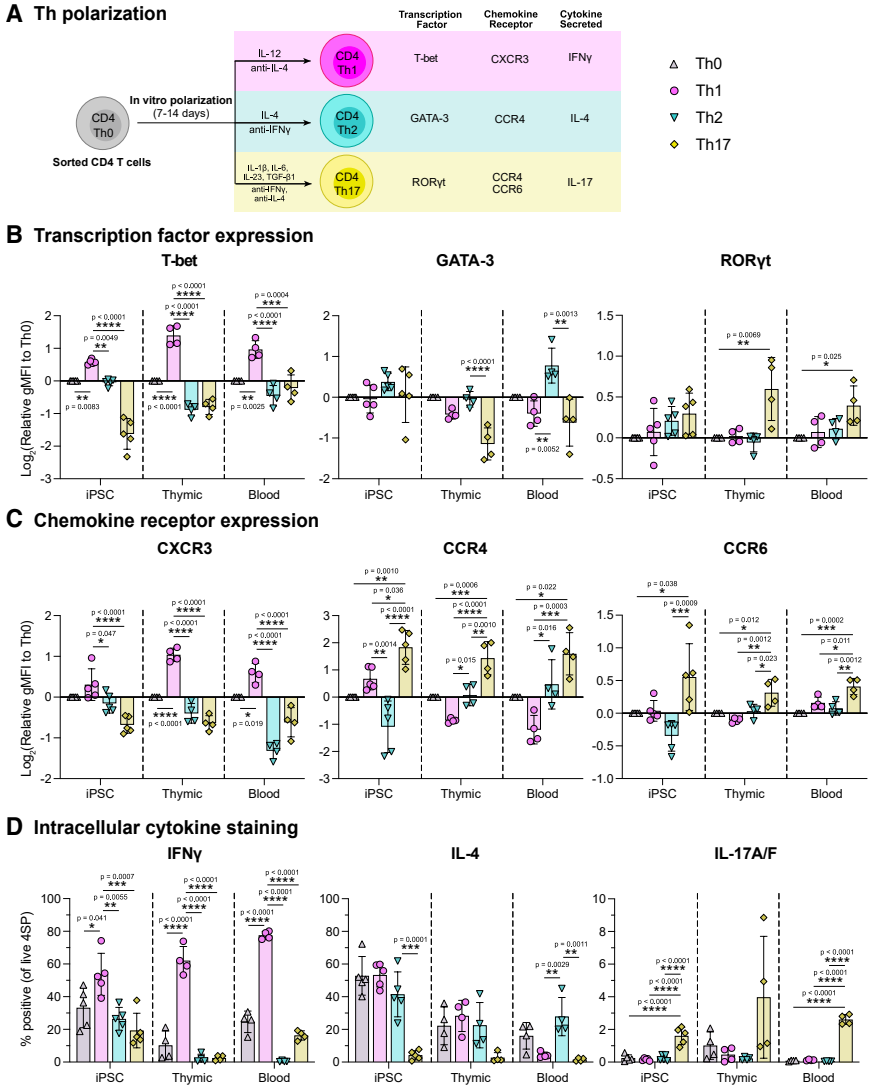


**Figure 7. iPSC-CD4$^+$ T cells can polarize into functionally different T helper subsets**

(A) Schematic of polarization conditions and relevant Th markers.

(B and C) TF and CR expression in CD4$^+$CD8α$^-$ cells. Relative gMFI values normalized to Th0 and then $\log_2$-transformed.

(D) Intracellular cytokine expression in CD4$^+$ CD8α$^-$ cells after stimulation with PMA, Iono, and brefeldin A.

For all plots, values are mean ± standard deviation; $n = 5$ differentiations or $n = 4$ thymic or blood donors; statistical significance was determined using ordinary one-way ANOVA followed by Tukey HSD test, with $p$ values shown. Detailed statistics are provided in Table S1.

See also Figure S7.

was most highly expressed in iPSC-Th1 cells, likely driving corresponding patterns of CXCR3 expression. Interestingly, iPSC- and thymic-Th cells uniformly expressed GATA-3 regardless of polarization condition, likely driving similarly broad CCR4 expression (Figure S7D).

We next investigated if polarized iPSC-Th cells produce hallmark Th cell cytokines (interferon [IFN]-γ for Th1; IL-4 for Th2; IL-17A/F for Th17). Th cells were stimulated with PMA + Iono in the presence of brefeldin A for 4 h and then stained for intracellular cytokine expression (Figures 7D and S7E). Under Th1 conditions, iPSC-Th1 cells significantly upregulated IFN-γ expression, compared with respective Th0, Th2, and Th17 conditions. Interestingly, neither iPSC- nor thymic-Th1 cells downregulated IL-4 expression relative to Th0, unlike blood-Th1 cells. Under Th2 conditions, IL-4 expression was unchanged from Th0 for all iPSC-, thymic-, and blood-Th2. Notably, IFN-γ was not suppressed in iPSC-Th2 cells, unlike thymic- and blood-Th2. Under Th17 conditions, iPSC-Th17 significantly upregulated IL-17A/F expression relative to other subsets and downregulated IFN-γ and IL-4 expression relative to iPSC- Th1 and -Th2, with a similar overall pattern of cytokine production like thymic- and blood-Th17 cells. Overall, these results indicate that TFs, CRs, and cytokine outputs of iPSC-CD4$^+$ T cells can be polarized toward states resembling canonical Th cell lineages.

## DISCUSSION

Throughout this work, we made several advances to better control development and maturation of PSC-derived CD4 vs. CD8 lineages. Optimization of TCR stimulation inputs better recapitulated the unique TCR signaling dynamics of CD4 vs. CD8 lineage induction, while modulating Notch signaling tuned TCR signaling kinetics and downstream induction of key proteins including ThPOK (CD4 lineage master regulator) and Nur77 (negative selection driver). Extending the DP-to-SP induction period from 1 to 2 weeks allowed time for more complete downregulation of CD8α in CD4 lineage-fated cells, while also increasing expression of naive T cell markers like CD45RA and CD62L. Naive marker expression was further reinforced by removing TCR signaling during the second week.[81] Our in-house media (PSC2) yields of ~0.5 CD4$^+$ T cells per input CD34$^+$ HE cell compare well with numbers from other studies producing iPSC-CD8$^+$ T cells in feeder- and serum-free conditions with non-commercial media and non-T cell-derived iPSCs.[11,13,14]

It is well known that *in vivo*, longer/stronger TCR stimulation generates CD4$^+$ T cells while shorter/weaker stimulation generates CD8$^+$ T cells.[82] However, it was unclear if artificial TCR stimulation modalities used for *in vitro* T cell maturation would recapitulate these behaviors. Unexpectedly, we found that high levels of some TCR pathway-stimulating reagents (anti-CD2/3/28, PHA) bias differentiation toward PSC-CD8$^+$ T cells, rather than the expected CD4$^+$ T cells. Our data suggest that this is due to a non-monotonic dose response between the input level of TCR-stimulating reagent and the output duration of TCR

pathway stimulation—too-low levels lead to insufficient induction of ThPOK and CD8 lineage bias; too-high levels lead to strong TCR downregulation and possibly higher induction of negative feedback regulators, which may interrupt TCR signaling similarly to CD8 downregulation following thymic TCR-pMHC class I interactions.[25] The need to optimize TCR stimulation might explain the lack of PSC-CD4$^+$ T cells in many published protocols, even when Notch ligands are not present in the DP-to-SP induction conditions.[11,64,83]

Our study demonstrates that Notch signaling specifically suppresses PSC-CD4$^+$ T cell induction. Previous work producing PSC-T cells in ATOs found that the use of MS5 feeder cells expressing DLL1, rather than the stronger DLL4, resulted in higher proportions and yields of mature CD4$^+$ T cells, although at the cost of reduced T cell yields overall.[33] These results suggest that weaker Notch ligands may be more permissive to *in vitro* PSC-CD4$^+$ T cell induction, although the effect could have been caused by an upstream change in cell development by DLL1 vs. DLL4. While the latter is still possible, our results show a definitive effect of Notch signaling during *in vitro* positive selection, whereby Notch ligands with increased strength of Notch1-mediated activation[34] (DLL4 > DLL1 > JAG2 ≈ JAG1 > no ligand) confer greater CD8 lineage bias. Since *NOTCH1*, *NOTCH2*, and *NOTCH3* are all expressed in our iPSC-DP cells, future work will be needed to dissect the individual and combinatorial contributions of each receptor toward CD8 lineage bias. As JAG1/2-based ATOs lead to poor PSC-T cell production,[38] appropriately timed DAPT administration during DLL4/DLL1 ATO cultures could unlock greater PSC-CD4$^+$ T cell generation in such systems. Finally, our findings suggest that suppression of DLL4 expression on cortical thymic epithelial cells by DP T cells *in vivo*[84] could be an important mechanism to prevent CD8 lineage bias.

Our data suggest that Notch signaling suppresses the PSC-CD4$^+$ T cell development primarily by suppressing TCR signaling and expression of the CD4 lineage TF ThPOK [*ZBTB7B*], enabling the CD8 lineage TF RUNX3 to dominate and bias differentiation toward CD8$^+$ T cells. The role of Notch signaling in *in vivo* DP-to-SP transition has been controversial, with studies showing CD4-biased, CD8-biased, or no bias following manipulation of Notch signaling.[31,32,85,86] Notably, our results are supported by a recent pre-print, in which CD4-conditional NICD1 overexpression in mice suppressed Gata3, Thpok, and subsequent 4SP development.[87] Our observation of Notch suppressing TCR stimulation in PSC-DP cells is consistent with an older model of NICD-overexpressing mice,[88] but it is in contrast to most literature in mature T cells showing Notch enhances TCR stimulation.[32,89,90] Thus, the effect of Notch on TCR stimulation is likely context and dose dependent.[32,88] In the case of strong TCR inputs that favor CD8 lineage induction, we hypothesize that Notch suppression of TCR signaling, especially induction of the pro-apoptosis protein Nur77 (*NR4A1*),[63] may serve to limit negative selection. We also observed increased IL7Rα expression during SP induction in the presence of Notch signaling, which may further support CD8 lineage induction.[25,57]

Through comparisons of TCR stimulating reagents, we saw striking differences in the effect of TCR-targeting reagents (anti-CD2/3/28 and PHA), compared with PMA+Iono, which bypasses the TCR to directly activate downstream pathways. The use of PMA to induce CD4$^+$ T cell development traces back to the first studies connecting TCR signaling strength to CD4 lineage commitment in *ex vivo* thymocytes.[26,91] The stronger CD4 bias of PMA+Iono likely stems in part from avoiding signal interruption by TCR downregulation and bypassing intermediate signaling nodes that may be affected by Notch signaling and/or differential activation of downstream pathways to favor ThPOK expression.[42] Additionally, while PMA induced the highest percent of CD4$^+$ T cells, anti-CD2/3/28 and PHA yielded more cells and better induced maturation markers (e.g., CD27, CD45RA, and CD62L). A recent publication reported PSC-CD4$^+$ T cell induction from T cell-derived iPSCs using PMA+Iono at a 10-fold higher PMA dose than we used, applied for 24 h rather than 1 to 2 weeks.[92] Consistent with our PMA+Iono results, their PSC-CD4$^+$ T cells were predominantly CD45RO$^+$CD62L$^-$, indicating either incomplete maturation or immediate differentiation. The poor induction of CD27 and CD45RA in our PMA+Iono-treated cells at any point after SP induction is consistent with the former possibility. Notably, we found that addition of anti-CD28 to PMA+Iono had no effect, indicating that lack of co-stimulation is not a limiting factor for PMA + Iono performance.

Through a combination of flow cytometry and CITE-seq/scTCR-seq, we demonstrated that PSC-CD4$^+$ T cells emerge from cells with diverse TCR clones, efficiently upregulate naive T cell markers, express relatively low levels of cytotoxicity genes, and retain memory-like phenotypes when expanded in IL-7/15 conditions. Functionally, the cells expressed co-stimulatory markers and polarized into Th1/2/17-like states, although less efficiently than blood T cells, and instead resembled extremely naive thymic CD4$^+$ T cells.

Overall, our results are a significant step forward in understanding and controlling PSC-T cell development. The ability to manufacture diverse types of Th cells opens the door to manufacturing therapeutic PSC-derived T cell products for a variety of diseases including cancer, autoimmunity, chronic inflammation, and transplant.[1–3] Our work will enable production of PSC-CAR-T products with defined ratios of CD4$^+$ and CD8$^+$ T cells, which is expected to improve clinical responses and patient outcomes in the treatment of cancer.[18,44] More broadly, the growing capability to reproduce the blood system from PSCs will enable modeling and exploration of human immune development *in vitro*,[74] production of isogenic cells for immune-competent tissue modeling,[93] and production of cell therapies comprising multiple cooperative immune cell types.[94]

## Limitations of the study

A general challenge in PSC-T cell production is variable yields and quality of upstream HSPCs, especially when adapting blood induction protocols to new PSC lines, which strongly affects downstream PSC-T cell production purities and yields. In addition, the removal of Notch signaling for PSC-CD4$^+$ T cell induction is timing-sensitive; since Notch is critical for earlier stages of T cell development, the cell population must achieve a high frequency of TCRαβ$^+$ DP cells, a stage at which Notch signaling is less essential,[95] to limit loss of cellularity when removing or inhibiting Notch. As cellularity is generally lost during SP induction, additional media optimization could improve cell survival and purity of SP populations. The reduced expansion of

PSC-CD4$^+$ T cells relative to primary T cells may indicate the need for further maturation after SP induction. Further maturation may also help to suppress aberrant CD8 or CD4 re-expression during expansion and polarization, as well as improve control over polarization itself.

In terms of function, future studies will be needed to determine whether cytokine outputs from polarized PSC-Th subtypes are sufficient to control the function of other immune cells. It also remains to be established whether these cells will persist and maintain their phenotype and function in an *in vivo* environment and which ratios and polarization states of PSC-CD4$^+$ and CD8$^+$ T cells are best to treat different cancers and infectious diseases, among other applications. Further, our use of CITE-seq proteins to approximate gated SP populations is prone to technical challenges, especially dropouts; future studies of sorted populations would improve analytical precision. Finally, while we used fibroblast-derived iPSCs to demonstrate robustness of our T cell and SP induction protocols, the resulting randomly generated TCR repertoire would pose a risk of alloreactivity and possible graft vs. host disease. For targeted therapies using PSC-T cells, future work should test our CD4$^+$ T cell induction protocol with reprogrammed T cells[64,96] or PSCs engineered to express specific antigen receptors and to prevent random TCR formation.[11,38] Except in cases where the TCR/CD3 complex is absent,[38] which may require additional optimization, we anticipate a high likelihood of success for diverse antigen receptors.

## RESOURCE AVAILABILITY

### Lead contact

Further information and requests for reagents and resources should be directed to and will be fulfilled by the lead contact, Peter W. Zandstra (peter.zandstra@ubc.ca).

### Materials availability

Custom CODEX antibodies are available from the lead contact upon request.

### Data and code availability

- CITE-seq and scTCR-seq data are available in Mendeley Data: https://doi.org/10.17632/k3xtwnzpyn.1.
- Sequencing analysis notebooks are available on GitHub and archived on Zenodo (Figures S1F and S1G: https://github.com/stemcellbioengineering/stankiewicz-michaels-M14, https://doi.org/10.5281/zenodo.17861714; Figures 5, 6, and S6: https://github.com/stemcellbioengineering/jones-salim-cd4, https://doi.org/10.5281/zenodo.17861549).
- Any additional information required to reanalyze the data reported in this paper is available from the lead contact upon request.

## ACKNOWLEDGMENTS

We thank thymus donors and their families, and surgical staff and coordinators at BC Children's Hospital for contributing to this research. We thank: Dr. Sabine Ivison for logistical support in thymus collection; Dr. Andreas Tiffeau-Meyer for helpful discussion of TCR sequencing analysis; Grace Kuo and Dr. Kelly McNagny for help annotating innate cell types in the CITE-seq dataset; Dr. Dominic Boardman and Rosa Garcia for advising on Th polarization experiments; and Laura Gonzalez for the RT-qPCR protocol and related advice. We acknowledge: SBME Sequencing Core for sequencing support; BRC Antibody Lab for technical support and custom reagents; and UBC and BCCHR Flow Cores for flow cytometry and sorting support. Certain figure cartoons were made with BioRender.

Funding for this work was provided by Genome BC (SIP031 to P.W.Z. and F.M.V.R.) and the Wellcome Leap Human Organs, Physiology, and Engineering (HOPE) program (AWD-017859 to P.W.Z., M.K.L., and F.M.V.R.), the Canadian Foundation for Innovation/B.C. Knowledge Development Fund (John Evans Leader's Fund 38395 to F.M.V.R), and the Canadian Institutes of Health Research (CIHR; ICC-17644 to M.K.L). R.D.J. is supported by a Michael Smith Health Research BC trainee award (RT-2021-1946) and an MSL Pathway to Independence Award. K.S. is supported by a CIHR Canadian Graduate Scholarship – Master's (CGS-M) and Doctoral (CGS-D) award and UBC Faculty of Medicine Graduate Student award. L.N.S. is supported by a National Sciences and Engineering Research Council of Canada (NSERC) CGS-D award. F.M.V.R. is supported by the CIHR (FDN-159908). M.K.L. is a Canada Research Chair in Engineered Immune Tolerance and receives a Scientist Salary Award from the BC Children's Hospital Research Institute. P.W.Z. is a Canada Research Chair in Stem Cell Bioengineering.

## AUTHOR CONTRIBUTIONS

Conceptualization and methodology: R.D.J., K.S., J.M.E., M.K.L., and P.W.Z.; investigation: R.D.J., K.S., J.M.E., L.L., J.K.G., A.M., L.J.D., C.L., T.P.B.T., H.H.H., and Y.S.M.; resources: T.P.B.T., H.H.H., and C.Z.; data curation, formal analysis, and visualization: R.D.J., K.S., L.N.S., and D.R.; writing – original draft: R.D.J., K.S., and L.N.S.; writing – reviewing & editing: R.D.J., K.S., L.N.S., M.K.L., and P.W.Z.; supervision and project administration: M.K.L. and P.W.Z.; funding acquisition: F.M.V.R., M.K.L., and P.W.Z.

## DECLARATION OF INTERESTS

The University of British Columbia has filed a patent application related to this work on behalf of the authors.

## STAR★METHODS

Detailed methods are provided in the online version of this paper and include the following:

- KEY RESOURCES TABLE
- EXPERIMENTAL MODEL AND STUDY PARTICIPANT DETAILS
  - Human pluripotent stem cell (hPSC) lines
  - Patient samples
- METHOD DETAILS
  - CODEX image analysis of Notch ligand density in postnatal thymus
  - PSC to HE differentiation
  - PSC-HE to DP T cell differentiation
  - PSC-DP to SP T cell differentiation
  - PSC-CD4$^+$ T cell generation and isolation for expansion and polarization tests
  - CD4$^+$ T cell isolation from human postnatal thymus
  - CD4$^+$ T cell isolation from human adult peripheral blood
  - T cell expansion and polarization
  - T cell proliferation, activation assay and intracellular cytokine staining
  - Flow cytometry
  - RT-qPCR
  - Sample preparations for CITE-seq
  - CITE-seq data processing and analysis
  - Signature gene collation and scoring
  - TCR repertoire analysis
- QUANTIFICATION AND STATISTICAL ANALYSIS
  - Multi-way ANOVA

## SUPPLEMENTAL INFORMATION

Supplemental information can be found online at https://doi.org/10.1016/j.stem.2025.12.010.

Received: October 29, 2024
Revised: October 1, 2025
Accepted: December 9, 2025
Published: January 8, 2026

## REFERENCES

1. Rosado-Sánchez, I., and Levings, M.K. (2020). Building a CAR-Treg: Going from the basic to the luxury model. Cell. Immunol. *358*, 104220. https://doi.org/10.1016/j.cellimm.2020.104220.
2. Schett, G., Müller, F., Taubmann, J., Mackensen, A., Wang, W., Furie, R.A., Gold, R., Haghikia, A., Merkel, P.A., Caricchio, R., et al. (2024). Advancements and challenges in CAR T cell therapy in autoimmune diseases. Nat. Rev. Rheumatol. *20*, 531–544. https://doi.org/10.1038/s41584-024-01139-z.
3. Aghajanian, H., Rurik, J.G., and Epstein, J.A. (2022). CAR-based therapies: opportunities for immuno-medicine beyond cancer. Nat. Metab. *4*, 163–169. https://doi.org/10.1038/s42255-022-00537-5.
4. Martin, K.E., Hammer, Q., Perica, K., Sadelain, M., and Malmberg, K.J. (2024). Engineering immune-evasive allogeneic cellular immunotherapies. Nat. Rev. Immunol. *24*, 680–693. https://doi.org/10.1038/s41577-024-01022-8.
5. Depil, S., Duchateau, P., Grupp, S.A., Mufti, G., and Poirot, L. (2020). 'Off-the-shelf' allogeneic CAR T cells: development and challenges. Nat. Rev. Drug Discov. *19*, 185–199. https://doi.org/10.1038/s41573-019-0051-2.
6. Michaels, Y.S., Durland, L.J., and Zandstra, P.W. (2023). Engineering T Cell Development for the Next Generation of Stem Cell-Derived Immunotherapies. GEN Biotechnol. *2*, 106–119. https://doi.org/10.1089/genbio.2023.0008.
7. Timmermans, F., Velghe, I., Vanwalleghem, L., De Smedt, M., Van Coppernolle, S., Taghon, T., Moore, H.D., Leclercq, G., Langerak, A.W., Kerre, T., et al. (2009). Generation of T Cells from Human Embryonic Stem Cell-Derived Hematopoietic Zones. J. Immunol. *182*, 6879–6888. https://doi.org/10.4049/jimmunol.0803670.
8. Themeli, M., Kloss, C.C., Ciriello, G., Fedorov, V.D., Perna, F., Gonen, M., and Sadelain, M. (2013). Generation of tumor-targeted human T lymphocytes from induced pluripotent stem cells for cancer therapy. Nat. Biotechnol. *31*, 928–933. https://doi.org/10.1038/nbt.2678.
9. Nishimura, T., Kaneko, S., Kawana-Tachikawa, A., Tajima, Y., Goto, H., Zhu, D., Nakayama-Hosoya, K., Iriguchi, S., Uemura, Y., Shimizu, T., et al. (2013). Generation of rejuvenated antigen-specific T cells by reprogramming to pluripotency and redifferentiation. Cell Stem Cell *12*, 114–126. https://doi.org/10.1016/j.stem.2012.11.002.
10. Vizcardo, R., Masuda, K., Yamada, D., Ikawa, T., Shimizu, K., Fujii, S.I., Koseki, H., and Kawamoto, H. (2013). Regeneration of human tumor antigen-specific T cells from iPSCs derived from mature CD8(+) T cells. Cell Stem Cell *12*, 31–36. https://doi.org/10.1016/j.stem.2012.12.006.
11. Iriguchi, S., Yasui, Y., Kawai, Y., Arima, S., Kunitomo, M., Sato, T., Ueda, T., Minagawa, A., Mishima, Y., Yanagawa, N., et al. (2021). A clinically applicable and scalable method to regenerate T-cells from iPSCs for off-the-shelf T-cell immunotherapy. Nat. Commun. *12*, 430. https://doi.org/10.1038/s41467-020-20658-3.
12. Trotman-Grant, A.C., Mohtashami, M., De Sousa Casal, J., Martinez, E.C., Lee, D., Teichman, S., Brauer, P.M., Han, J., Anderson, M.K., and Zúñiga-Pflücker, J.C. (2021). DL4-μbeads induce T cell lineage differentiation from stem cells in a stromal cell-free system. Nat. Commun. *12*, 5023. https://doi.org/10.1038/s41467-021-25245-8.
13. Michaels, Y.S., Edgar, J.M., Major, M.C., Castle, E.L., Zimmerman, C., Yin, T., Hagner, A., Lau, C., Hsu, H.H., Ibañez-Rios, M.I., et al. (2022). DLL4 and VCAM1 enhance the emergence of T cell-competent hematopoietic progenitors from human pluripotent stem cells. Sci. Adv. *8*, eabn5522. https://doi.org/10.1126/sciadv.abn5522.
14. Jing, R., Scarfo, I., Najia, M.A., Lummertz da Rocha, E., Han, A., Sanborn, M., Bingham, T., Kubaczka, C., Jha, D.K., Falchetti, M., et al. (2022). EZH1 repression generates mature iPSC-derived CAR T cells with enhanced antitumor activity. Cell Stem Cell *29*, 1181–1196.e6. https://doi.org/10.1016/j.stem.2022.06.014.
15. Moeller, M., Haynes, N.M., Kershaw, M.H., Jackson, J.T., Teng, M.W.L., Street, S.E., Cerutti, L., Jane, S.M., Trapani, J.A., Smyth, M.J., et al. (2005). Adoptive transfer of gene-engineered CD4+ helper T cells induces potent primary and secondary tumor rejection. Blood *106*, 2995–3003. https://doi.org/10.1182/blood-2004-12-4906.
16. Moeller, M., Kershaw, M.H., Cameron, R., Westwood, J.A., Trapani, J.A., Smyth, M.J., and Darcy, P.K. (2007). Sustained antigen-specific antitumor recall response mediated by gene-modified CD4+ T helper-1 and CD8+ T cells. Cancer Res. *67*, 11428–11437. https://doi.org/10.1158/0008-5472.CAN-07-1141.
17. Sommermeyer, D., Hudecek, M., Kosasih, P.L., Gogishvili, T., Maloney, D.G., Turtle, C.J., and Riddell, S.R. (2016). Chimeric antigen receptor-modified T cells derived from defined CD8+ and CD4+ subsets confer superior antitumor reactivity in vivo. Leukemia *30*, 492–500. https://doi.org/10.1038/leu.2015.247.
18. Melenhorst, J.J., Chen, G.M., Wang, M., Porter, D.L., Chen, C., Collins, M.A., Gao, P., Bandyopadhyay, S., Sun, H., Zhao, Z., et al. (2022). Decade-long leukaemia remissions with persistence of CD4+ CAR T cells. Nature *602*, 503–509. https://doi.org/10.1038/s41586-021-04390-6.
19. He, Y., Hong, C., Huang, S., Kaskow, J.A., Covarrubias, G., Pires, I.S., Sacane, J.C., Hammond, P.T., and Belcher, A.M. (2023). STING Protein-Based In Situ Vaccine Synergizes CD4+ T, CD8+ T, and NK Cells for Tumor Eradication. Adv. Healthc. Mater. *12*, e2300688. https://doi.org/10.1002/adhm.202300688.
20. Zuazo, M., Arasanz, H., Bocanegra, A., Fernandez, G., Chocarro, L., Vera, R., Kochan, G., and Escors, D. (2020). Systemic CD4 Immunity as a Key Contributor to PD-L1/PD-1 Blockade Immunotherapy Efficacy. Front. Immunol. *11*, 586907. https://doi.org/10.3389/fimmu.2020.586907.
21. Zuazo, M., Arasanz, H., Fernández-Hinojal, G., García-Granda, M.J., Gato, M., Bocanegra, A., Martínez, M., Hernández, B., Teijeira, L., Morilla, I., et al. (2019). Functional systemic CD4 immunity is required for clinical responses to PD-L1/PD-1 blockade therapy. EMBO Mol. Med. *11*, e10293. https://doi.org/10.15252/emmm.201910293.
22. Van Hoecke, L., Van Lint, S., Roose, K., Van Parys, A., Vandenabeele, P., Grooten, J., Tavernier, J., De Koker, S., and Saelens, X. (2018). Treatment with mRNA coding for the necroptosis mediator MLKL induces antitumor immunity directed against neo-epitopes. Nat. Commun. *9*, 3417. https://doi.org/10.1038/s41467-018-05979-8.
23. Cardenas, M.A., Prokhnevska, N., Sobierajska, E., Gregorova, P., Medina, C.B., Valanparambil, R.M., Greenwald, R., DelBalzo, L., Bilen, M.A., Joshi, S.S., et al. (2024). Differentiation fate of a stem-like CD4 T cell controls immunity to cancer. Nature *636*, 224–232. https://doi.org/10.1038/s41586-024-08076-7.
24. Shinzawa, M., Moseman, E.A., Gossa, S., Mano, Y., Bhattacharya, A., Guinter, T., Alag, A., Chen, X., Cam, M., McGavern, D.B., et al. (2022). Reversal of the T cell immune system reveals the molecular basis for T cell lineage fate determination in the thymus. Nat. Immunol. *23*, 731–742. https://doi.org/10.1038/s41590-022-01187-1.
25. Singer, A., Adoro, S., and Park, J.H. (2008). Lineage fate and intense debate: Myths, models and mechanisms of CD4- versus CD8-lineage choice. Nat. Rev. Immunol. *8*, 788–801. https://doi.org/10.1038/nri2416.
26. Iwata, M., Kuwata, T., Mukai, M., Tozawa, Y., and Yokoyama, M. (1996). Differential induction of helper and killer T cells from isolated CD4+CD8+ thymocytes in suspension culture. Eur. J. Immunol. *26*, 2081–2086. https://doi.org/10.1002/eji.1830260918.
27. Yasutomo, K., Doyle, C., Miele, L., Fuchs, C., and Germain, R.N. (2000). The duration of antigen receptor signalling determines CD4+ versus CD8+ T-cell lineage fate. Nature *404*, 506–510. https://doi.org/10.1038/35006664.

28. Steier, Z., Kim, E.J.Y., Aylard, D.A., and Robey, E.A. (2024). The CD4 Versus CD8 T Cell Fate Decision: A Multiomics-Informed Perspective. Annu. Rev. Immunol. *42*, 235–258. https://doi.org/10.1146/annurev-immunol-083122-040929.

29. He, X., He, X., Dave, V.P., Zhang, Y., Hua, X., Nicolas, E., Xu, W., Roe, B.A., and Kappes, D.J. (2005). The zinc finger transcription factor Th-POK regulates CD4 versus CD8 T-cell lineage commitment. Nature *433*, 826–833. https://doi.org/10.1038/nature03338.

30. Sun, G., Liu, X., Mercado, P., Jenkinson, S.R., Kypriotou, M., Feigenbaum, L., Galéra, P., and Bosselut, R. (2005). The zinc finger protein cKrox directs CD4 lineage differentiation during intrathymic T cell positive selection. Nat. Immunol. *6*, 373–381. https://doi.org/10.1038/ni1183.

31. Laky, K., Fleischacker, C., and Fowlkes, B.J. (2006). TCR and Notch signaling in CD4 and CD8 T-cell development. Immunol. Rev. *209*, 274–283. https://doi.org/10.1111/j.0105-2896.2006.00358.x.

32. Laky, K., and Fowlkes, B.J. (2008). Notch signaling in CD4 and CD8 T cell development. Curr. Opin. Immunol. *20*, 197–202. https://doi.org/10.1016/j.coi.2008.03.004.

33. Montel-Hagen, A., Seet, C.S., Li, S., Chick, B., Zhu, Y., Chang, P., Tsai, S., Sun, V., Lopez, S., Chen, H.C., et al. (2019). Organoid-Induced Differentiation of Conventional T Cells from Human Pluripotent Stem Cells. Cell Stem Cell *24*, 376–389.e8. https://doi.org/10.1016/j.stem.2018.12.011.

34. Van De Walle, I., De Smet, G., Gärtner, M., De Smedt, M., Waegemans, E., Vandekerckhove, B., Leclercq, G., Plum, J., Aster, J.C., Bernstein, I.D., et al. (2011). Jagged2 acts as a Delta-like Notch ligand during early hematopoietic cell fate decisions. Blood *117*, 4449–4459. https://doi.org/10.1182/blood-2010-06-290049.

35. Michaels, Y.S., Major, M.C., Bonham-Carter, B., Zhang, J., Heydari, T., Edgar, J.M., Siu, M.M., Greenstreet, L., Vilarrasa-Blasi, R., Kim, S., et al. (2024). Tracking the gene expression programs and clonal relationships that underlie mast, myeloid, and T lineage specification from stem cells. Cell Syst. *15*, 1245–1263.e10. https://doi.org/10.1016/j.cels.2024.11.001.

36. Vanhecke, D., Verhasselt, B., De Smedt, M., Leclercq, G., Plum, J., and Vandekerckhove, B. (1997). Human thymocytes become lineage committed at an early postselection CD69+ stage, before the onset of functional maturation. J. Immunol. *159*, 5973–5983. https://doi.org/10.4049/jimmunol.159.12.5973.

37. Stankiewicz, L.N., Salim, K., Flaschner, E.A., Wang, Y.X., Edgar, J.M., Durland, L.J., Lin, B.Z.B., Bingham, G.C., Major, M.C., Jones, R.D., et al. (2024). Sex-biased human thymic architecture guides T cell development through spatially defined niches. Dev. Cell *60*, 152–169.e8. https://doi.org/10.1016/j.devcel.2024.09.011.

38. van der Stegen, S.J.C., Lindenbergh, P.L., Petrovic, R.M., Xie, H., Diop, M.P., Alexeeva, V., Shi, Y., Mansilla-Soto, J., Hamieh, M., Eyquem, J., et al. (2022). Generation of T-cell-receptor-negative CD8αβ-positive CAR T cells from T-cell-derived induced pluripotent stem cells. Nat. Biomed. Eng. *6*, 1284–1297. https://doi.org/10.1038/s41551-022-00915-0.

39. Mohtashami, M., Shah, D.K., Nakase, H., Kianizad, K., Petrie, H.T., and Zúñiga-Pflücker, J.C. (2010). Direct Comparison of Dll1- and Dll4-Mediated Notch Activation Levels Shows Differential Lymphomyeloid Lineage Commitment Outcomes. J. Immunol. *185*, 867–876. https://doi.org/10.4049/jimmunol.1000782.

40. Kuintzle, R., Santat, L.A., and Elowitz, M.B. (2025). Diversity in Notch ligand-receptor signaling interactions. eLife *12*, RP91422. https://doi.org/10.7554/eLife.91422.

41. Van de Walle, I., Waegemans, E., De Medts, J., De Smet, G., De Smedt, M., Snauwaert, S., Vandekerckhove, B., Kerre, T., Leclercq, G., Plum, J., et al. (2013). Specific Notch receptor-ligand interactions control human TCR-αβ/γδ development by inducing differential Notch signal strength. J. Exp. Med. *210*, 683–697. https://doi.org/10.1084/jem.20121798.

42. Steier, Z., Aylard, D.A., McIntyre, L.L., Baldwin, I., Kim, E.J.Y., Lutes, L.K., Ergen, C., Huang, T.-S., Robey, E.A., Yosef, N., et al. (2023). Single-cell multiomic analysis of thymocyte development reveals drivers of CD4+ T cell and CD8+ T cell lineage commitment. Nat. Immunol. *24*, 1579–1590. https://doi.org/10.1038/s41590-023-01584-0.

43. Chopp, L.B., Gopalan, V., Ciucci, T., Ruchinskas, A., Rae, Z., Lagarde, M., Gao, Y., Li, C., Bosticardo, M., Pala, F., et al. (2020). An Integrated Epigenomic and Transcriptomic Map of Mouse and Human αβ T Cell Development. Immunity *53*, 1182–1201.e8. https://doi.org/10.1016/j.immuni.2020.10.024.

44. Cohen, A.D., Garfall, A.L., Stadtmauer, E.A., Melenhorst, J.J., Lacey, S.F., Lancaster, E., Vogl, D.T., Weiss, B.M., Dengel, K., Nelson, A., et al. (2019). B cell maturation antigen-specific CAR T cells are clinically active in multiple myeloma. J. Clin. Investig. *129*, 2210–2221. https://doi.org/10.1172/JCI126397.

45. Karimi, M.M., Guo, Y., Cui, X., Pallikonda, H.A., Horková, V., Wang, Y.F., Gil, S.R., Rodriguez-Esteban, G., Robles-Rebollo, I., Bruno, L., et al. (2021). The order and logic of CD4 versus CD8 lineage choice and differentiation in mouse thymus. Nat. Commun. *12*, 99. https://doi.org/10.1038/s41467-020-20306-w.

46. Taniuchi, I. (2018). CD4 Helper and CD8 Cytotoxic T Cell Differentiation. Annu. Rev. Immunol. *36*, 579–601. https://doi.org/10.1146/annurev-immunol-042617-053411.

47. Naito, T., and Taniuchi, I. (2010). The network of transcription factors that underlie the CD4 versus CD8 lineage decision. Int. Immunol. *22*, 791–796. https://doi.org/10.1093/intimm/dxq436.

48. Vacchio, M.S., and Bosselut, R. (2016). What Happens in the Thymus Does Not Stay in the Thymus: How T Cells Recycle the CD4+ – CD8+ Lineage Commitment Transcriptional Circuitry To Control Their Function. J. Immunol. *196*, 4848–4856. https://doi.org/10.4049/jimmunol.1600415.

49. Wang, L., and Bosselut, R. (2009). CD4-CD8 Lineage Differentiation: Thpok-ing into the Nucleus. J. Immunol. *183*, 2903–2910. https://doi.org/10.4049/jimmunol.0901041.

50. Baldwin, I., and Robey, E.A. (2024). Adjusting to self in the thymus: CD4 versus CD8 lineage commitment and regulatory T cell development. J. Exp. Med. *221*, e20230896. https://doi.org/10.1084/jem.20230896.

51. Trendel, N., Kruger, P., Gaglione, S., Nguyen, J., Pettmann, J., Sontag, E.D., and Dushek, O. (2021). Perfect adaptation of CD8+ T cell responses to constant antigen input over a wide range of affinities is overcome by costimulation. Sci. Signal. *14*, eaay9363. https://doi.org/10.1126/scisignal.aay9363.

52. Naramura, M., Jang, I.K., Kole, H., Huang, F., Haines, D., and Gu, H. (2002). C-Cbl and Cbl-b regulate T cell responsiveness by promoting ligand-induced TCR down-modulation. Nat. Immunol. *3*, 1192–1199. https://doi.org/10.1038/ni855.

53. Tanzola, M.B., and Kersh, G.J. (2006). The dual specificity phosphatase transcriptome of the murine thymus. Mol. Immunol. *43*, 754–762. https://doi.org/10.1016/j.molimm.2005.03.006.

54. Voisinne, G., Gonzalez de Peredo, A., and Roncagalli, R. (2018). CD5, an Undercover Regulator of TCR Signaling. Front. Immunol. *9*, 2900. https://doi.org/10.3389/fimmu.2018.02900.

55. Amsen, D., Helbig, C., and Backer, R.A. (2015). Notch in T Cell Differentiation: All Things Considered. Trends Immunol. *36*, 802–814. https://doi.org/10.1016/j.it.2015.10.007.

56. Rafei, M., Rouette, A., Brochu, S., Vanegas, J.R., and Perreault, C. (2013). Differential effects of γc cytokines on postselection differentiation of CD8 thymocytes. Blood *121*, 107–117. https://doi.org/10.1182/blood-2012-05-433508.

57. Etzensperger, R., Kadakia, T., Tai, X., Alag, A., Guinter, T.I., Egawa, T., Erman, B., and Singer, A. (2017). Identification of lineage-specifying cytokines that signal all CD8+-cytotoxic-lineage-fate "decisions" in the thymus. Nat. Immunol. *18*, 1218–1227. https://doi.org/10.1038/ni.3847.

58. Wang, L., Wildt, K.F., Zhu, J., Zhang, X., Feigenbaum, L., Tessarollo, L., Paul, W.E., Fowlkes, B.J., and Bosselut, R. (2008). Distinct functions for the transcription factors GATA-3 and ThPOK during intrathymic differentiation of CD4+ T cells. Nat. Immunol. *9*, 1122–1130. https://doi.org/10.1038/ni.1647.

59. Xiong, Y., Castro, E., Yagi, R., Zhu, J., Lesourne, R., Love, P.E., Feigenbaum, L., and Bosselut, R. (2013). Thpok-independent repression of Runx3 by Gata3 during CD4+ T-cell differentiation in the thymus. Eur. J. Immunol. *43*, 918–928. https://doi.org/10.1002/eji.201242944.

60. Gimferrer, I., Hu, T., Simmons, A., Wang, C., Souabni, A., Busslinger, M., Bender, T.P., Hernandez-Hoyos, G., and Alberola-Ila, J. (2011). Regulation of GATA-3 Expression during CD4 Lineage Differentiation. J. Immunol. *186*, 3892–3898. https://doi.org/10.4049/jimmunol.1003505.

61. Rui, J., Liu, H., Zhu, X., Cui, Y., and Liu, X. (2012). Epigenetic Silencing of Cd8 Genes by ThPOK-Mediated Deacetylation during CD4 T Cell Differentiation. J. Immunol. *189*, 1380–1390. https://doi.org/10.4049/jimmunol.1201077.

62. Sato, T., Ohno, S.I., Hayashi, T., Sato, C., Kohu, K., Satake, M., and Habu, S. (2005). Dual functions of runx proteins for reactivating CD8 and silencing CD4 at the commitment process into CD8 thymocytes. Immunity *22*, 317–328. https://doi.org/10.1016/j.immuni.2005.01.012.

63. Jehn, B.M., Bielke, W., Pear, W.S., and Osborne, B.A. (1999). Cutting Edge: Protective Effects of Notch-1 on TCR-Induced Apoptosis. J. Immunol. *162*, 635–638. https://doi.org/10.4049/jimmunol.162.2.635.

64. Kawai, Y., Kawana-Tachikawa, A., Kitayama, S., Ueda, T., Miki, S., Watanabe, A., and Kaneko, S. (2021). Generation of highly proliferative, rejuvenated cytotoxic T cell clones through pluripotency reprogramming for adoptive immunotherapy. Mol. Ther. *29*, 3027–3041. https://doi.org/10.1016/j.ymthe.2021.05.016.

65. Traag, V.A., Waltman, L., and van Eck, N.J. (2019). From Louvain to Leiden: guaranteeing well-connected communities. Sci. Rep. *9*, 5233. https://doi.org/10.1038/s41598-019-41695-z.

66. Mazziotta, F., Martin, L.E., Egan, D.N., Bar, M., Kinsella, S., Paulson, K.G., Voillet, V., Lahman, M.C., Hunter, D., Schmitt, T.M., et al. (2025). A phase I/II trial of WT1-specific TCR gene therapy for patients with acute myeloid leukemia and active disease post-allogeneic hematopoietic cell transplantation: skewing towards NK-like phenotype impairs T cell function and persistence. Nat. Commun. *16*, 5214. https://doi.org/10.1038/s41467-025-60394-0.

67. Mulè, M.P., Martins, A.J., and Tsang, J.S. (2022). Normalizing and denoising protein expression data from droplet-based single cell profiling. Nat. Commun. *13*, 2099. https://doi.org/10.1038/s41467-022-29356-8.

68. Oliaeimotlagh, M., Kumar, S., Taraskin, A., Armstrong Suthahar, S.S., Suryawanshi, V., Chiang, A.W.T., and Ley, K. (2025). Automated denoising of CITE-seq data with ThresholdR. Cell Rep. Methods *5*, 101088. https://doi.org/10.1016/j.crmeth.2025.101088.

69. Park, J.E., Botting, R.A., Domínguez Conde, C.D., Popescu, D.M., Lavaert, M., Kunz, D.J., Goh, I., Stephenson, E., Ragazzini, R., Tuck, E., et al. (2020). A cell atlas of human thymic development defines T cell repertoire formation. Science *367*, eaay3224. https://doi.org/10.1126/science.aay3224.

70. Suo, C., Dann, E., Goh, I., Jardine, L., Kleshchevnikov, V., Park, J.E., Botting, R.A., Stephenson, E., Engelbert, J., Tuong, Z.K., et al. (2022). Mapping the developing human immune system across organs. Science *376*, eabo0510. https://doi.org/10.1126/science.abo0510.

71. Slauenwhite, D., and Johnston, B. (2015). Regulation of NKT cell localization in homeostasis and infection. Front. Immunol. *6*, 255. https://doi.org/10.3389/fimmu.2015.00255.

72. Abramowski, P., Ogrodowczyk, C., Martin, R., and Pongs, O. (2014). A truncation variant of the cation channel P2RX5 is upregulated during T cell activation. PLoS One *9*, e104692. https://doi.org/10.1371/journal.pone.0104692.

73. Fontana, M.F., de Melo, G.L., Anidi, C., Hamburger, R., Kim, C.Y., Lee, S.Y., Pham, J., and Kim, C.C. (2016). Macrophage Colony Stimulating Factor Derived from CD4+ T Cells Contributes to Control of a Blood-Borne Infection. PLoS Pathog. *12*, e1006046. https://doi.org/10.1371/journal.ppat.1006046.

74. Stankiewicz, L.N., Rossi, F.M.V., and Zandstra, P.W. (2024). Rebuilding and rebooting immunity with stem cells. Cell Stem Cell *31*, 597–616. https://doi.org/10.1016/j.stem.2024.03.012.

75. Park, J.J., Lee, K.A.V., Lam, S.Z., Moon, K.S., Fang, Z., and Chen, S. (2023). Machine learning identifies T cell receptor repertoire signatures associated with COVID-19 severity. Commun. Biol. *6*, 76. https://doi.org/10.1038/s42003-023-04447-4.

76. Trofimov, A., Brouillard, P., Larouche, J.D., Séguin, J., Laverdure, J.P., Brasey, A., Ehx, G., Roy, D.C., Busque, L., Lachance, S., et al. (2022). Two types of human TCR differentially regulate reactivity to self and non-self antigens. iScience *25*, 104968. https://doi.org/10.1016/j.isci.2022.104968.

77. Tiffeau-Mayer, A. (2024). Unbiased estimation of sampling variance for Simpson's diversity index. Phys. Rev. E *109*, 064411. https://doi.org/10.1103/PhysRevE.109.064411.

78. Carico, Z.M., Roy Choudhury, K., Zhang, B., Zhuang, Y., and Krangel, M.S. (2017). Tcrd Rearrangement Redirects a Processive Tcra Recombination Program to Expand the Tcra Repertoire. Cell Rep. *19*, 2157–2173. https://doi.org/10.1016/j.celrep.2017.05.045.

79. Zielinski, C.E. (2023). T helper cell subsets: diversification of the field. Eur. J. Immunol. *53*, e2250218. https://doi.org/10.1002/eji.202250218.

80. Boardman, D.A., Garcia, R.V., Ivison, S.M., Bressler, B., Dhar, T.M., Zhao, Q., and Levings, M.K. (2020). Pharmacological inhibition of RORC2 enhances human Th17-Treg stability and function. Eur. J. Immunol. *50*, 1400–1411. https://doi.org/10.1002/eji.201948435.

81. Love, P.E., and Bhandoola, A. (2011). Signal integration and crosstalk during thymocyte migration and emigration. Nat. Rev. Immunol. *11*, 469–477. https://doi.org/10.1038/nri2989.

82. Taniuchi, I. (2018). CD4 helper and CD8 cytotoxic T cell differentiation. Annu. Rev. Immunol. *36*, 579–601. https://doi.org/10.1146/annurev-immunol-042617-053411.

83. Maeda, T., Nagano, S., Ichise, H., Kataoka, K., Yamada, D., Ogawa, S., Koseki, H., Kitawaki, T., Kadowaki, N., Takaori-Kondo, A., et al. (2016). Regeneration of CD8αβ T cells from T-cell-derived iPSC imparts potent tumor antigen-specific cytotoxicity. Cancer Res. *76*, 6839–6850. https://doi.org/10.1158/0008-5472.CAN-16-1149.

84. Fiorini, E., Ferrero, I., Merck, E., Favre, S., Pierres, M., Luther, S.A., and MacDonald, H.R. (2008). Cutting Edge: Thymic Crosstalk Regulates Delta-Like 4 Expression on Cortical Epithelial Cells. J. Immunol. *181*, 8199–8203. https://doi.org/10.4049/jimmunol.181.12.8199.

85. Robey, E., Chang, D., Itano, A., Cado, D., Alexander, H., Lans, D., Weinmaster, G., and Salmon, P. (1996). An activated form of Notch influences the choice between CD4 and CD8 T cell lineages. Cell *87*, 483–492. https://doi.org/10.1016/S0092-8674(00)81368-9.

86. Tanigaki, K., Tsuji, M., Yamamoto, N., Han, H., Tsukada, J., Inoue, H., Kubo, M., and Honjo, T. (2004). Regulation of αβ/γδ T cell lineage commitment and peripheral T cell responses by Notch/RBP-J signaling. Immunity *20*, 611–622. https://doi.org/10.1016/S1074-7613(04)00109-8.

87. El-Maklizi, M., Kousis, P.C., Yuan, J.S., Macdonald, B., Gower, M., Gams, M.S., Boudil, A., and Guidos, C.J. (2025). Activated Notch1 Redirects CD4-Fated CD4+ CD8+ Precursors to the CD8 Lineage During Thymocyte Selection Without Causing T Cell Leukemia. Preprint at bioRxiv. https://doi.org/10.1101/2025.02.28.640858.

88. Izon, D.J., Punt, J.A., Xu, L., Karnell, F.G., Allman, D., Myung, P.S., Boerth, N.J., Pui, J.C., Koretzky, G.A., and Pear, W.S. (2001). Notch1 regulates maturation of CD4+ and CD8+ thymocytes by modulating TCR signal strength. Immunity *14*, 253–264. https://doi.org/10.1016/S1074-7613(01)00107-8.

89. Steinbuck, M.P., Arakcheeva, K., and Winandy, S. (2018). Novel TCR-Mediated Mechanisms of Notch Activation and Signaling. J. Immunol. *200*, 997–1007. https://doi.org/10.4049/jimmunol.1700070.

90. Laky, K., Evans, S., Perez-Diez, A., and Fowlkes, B.J. (2015). Notch Signaling Regulates Antigen Sensitivity of Naive CD4+ T Cells by Tuning Co-stimulation. Immunity *42*, 80–94. https://doi.org/10.1016/j.immuni.2014.12.027.

91. Ohoka, Y., Kuwata, T., Tozawa, Y., Zhao, Y., Mukai, M., Motegi, Y., Suzuki, R., Yokoyama, M., and Iwata, M. (1996). In vitro differentiation and commitment of CD4+ CD8+ thymocytes to the CD4 lineage, without TCR engagement. Int. Immunol. *8*, 297–306. https://doi.org/10.1093/intimm/8.3.297.

92. Fong, H., Mendel, M., Jascur, J., Najmi, L., Kim, K., Lew, G., Garimalla, S., Schock, S., Hu, J., Villegas, A.G., et al. (2025). A Serum- and Feeder-Free System to Generate CD4 and Regulatory T Cells from Human iPSCs. Stem Cells *43*, sxaf001. https://doi.org/10.1093/stmcls/sxaf001.

93. Michaels, Y.S., Buchanan, C.F., Gjorevski, N., and Moisan, A. (2023). Bioengineering translational models of lymphoid tissues. Nat. Rev. Bioeng. *1*, 731–748. https://doi.org/10.1038/s44222-023-00101-0.

94. Xue, D., Lu, S., Zhang, H., Zhang, L., Dai, Z., Kaufman, D.S., and Zhang, J. (2023). Induced pluripotent stem cell-derived engineered T cells, natural killer cells, macrophages, and dendritic cells in immunotherapy. Trends Biotechnol. *41*, 907–922. https://doi.org/10.1016/j.tibtech.2023.02.003.

95. Hosokawa, H., and Rothenberg, E.V. (2021). How transcription factors drive choice of the T cell fate. Nat. Rev. Immunol. *21*, 162–176. https://doi.org/10.1038/s41577-020-00426-6.

96. Minagawa, A., Yoshikawa, T., Yasukawa, M., Hotta, A., Kunitomo, M., Iriguchi, S., Takiguchi, M., Kassai, Y., Imai, E., Yasui, Y., et al. (2018). Enhancing T Cell Receptor Stability in Rejuvenated iPSC-Derived T Cells Improves Their Use in Cancer Immunotherapy. Cell Stem Cell *23*, 850–858.e4. https://doi.org/10.1016/j.stem.2018.10.005.

97. Shukla, S., Langley, M.A., Singh, J., Edgar, J.M., Mohtashami, M., Zúñiga-Pflücker, J.C., and Zandstra, P.W. (2017). Progenitor T-cell differentiation from hematopoietic stem cells using Delta-like-4 and VCAM-1. Nat. Methods *14*, 531–538. https://doi.org/10.1038/nmeth.4258.

98. Jia, B., Chen, J., Wang, Q., Sun, X., Han, J., Guastaldi, F., Xiang, S., Ye, Q., and He, Y. (2021). SIRT6 Promotes Osteogenic Differentiation of Adipose-Derived Mesenchymal Stem Cells Through Antagonizing DNMT1. Front. Cell Dev. Biol. *9*, 1–13. https://doi.org/10.3389/fcell.2021.648627.

99. De Decker, M., Lavaert, M., Roels, J., Tilleman, L., Vandekerckhove, B., Leclercq, G., Van Nieuwerburgh, F., Van Vlierberghe, P., and Taghon, T. (2021). HES1 and HES4 have non-redundant roles downstream of Notch during early human T-cell development. Haematologica *106*, 130–141. https://doi.org/10.3324/haematol.2019.226126.

100. Tel-Karthaus, N., Kers-Rebel, E.D., Looman, M.W., Ichinose, H., de Vries, C.J., and Ansems, M. (2018). Nuclear receptor Nur77 deficiency alters dendritic cell function. Front. Immunol. *9*, 1–14. https://doi.org/10.3389/fimmu.2018.01797.

101. Wang, Y.X., Holbrook, C.A., Hamilton, J.N., Garoussian, J., Afshar, M., Su, S., Schürch, C.M., Lee, M.Y., Goltsev, Y., Kundaje, A., et al.. A single cell spatial temporal atlas of skeletal muscle reveals cellular neighborhoods that orchestrate regeneration and become disrupted in aging. https://doi.org/10.1101/2022.06.10.494732.

102. Wolf, F.A., Angerer, P., and Theis, F.J. (2018). SCANPY: large-scale single-cell gene expression data analysis. Genome Biol *19*, 15. https://doi.org/10.1111/1462-2920.13787.

103. White, S., Quinn, J., Enzor, J., Staats, J., Mosier, S.M., Almarode, J., Denny, T.N., Weinhold, K.J., Ferrari, G., and Chan, C. (2021). FlowKit: A Python Toolkit for Integrated Manual and Automated Cytometry Analysis Workflows. Front. Immunol. *12*, 768541. https://doi.org/10.3389/fimmu.2021.768541.

104. Sturm, G., Szabo, T., Fotakis, G., Haider, M., Rieder, D., Trajanoski, Z., and Finotello, F. (2020). Sequence analysis Scirpy: a Scanpy extension for analyzing single-cell T-cell receptor-sequencing data. Bioinformatics *36*, 4817–4818. https://doi.org/10.1093/bioinformatics/btaa611.

105. Thomson, J.A., Itskovitz-Eldor, J., Shapiro, S.S., Waknitz, M.A., Swiergiel, J.J., Marshall, V.S., and Jones, J.M. (1998). Embryonic stem cell lines derived from human blastocysts. Science *282*, 1145–1147. https://doi.org/10.1126/science.282.5391.1145.

106. Ditadi, A., Sturgeon, C.M., Tober, J., Awong, G., Kennedy, M., Yzaguirre, A.D., Azzola, L., Ng, E.S., Stanley, E.G., French, D.L., et al. (2015). Human definitive haemogenic endothelium and arterial vascular endothelium represent distinct lineages. Nat. Cell Biol. *17*, 580–591. https://doi.org/10.1038/ncb3161.

107. Schmiedel, B.J., Singh, D., Madrigal, A., Valdovino-Gonzalez, A.G., White, B.M., Zapardiel-Gonzalo, J., Ha, B., Altay, G., Greenbaum, J.A., McVicker, G., et al. (2018). Impact of Genetic Polymorphisms on Human Immune Cell Gene Expression. Cell *175*, 1701–1715.e16. https://doi.org/10.1016/j.cell.2018.10.022.

108. Tirosh, I., Izar, B., Prakadan, S.M., Wadsworth, M.H., Treacy, D., Trombetta, J.J., Rotem, A., Rodman, C., Lian, C., Murphy, G., et al. (2016). Dissecting the multicellular ecosystem of metastatic melanoma by single-cell RNA-seq. Science *352*, 189–196. https://doi.org/10.1126/science.aad0501.

109. Simpson, E.H. (1949). Measurement of Diversity. Nature *163*, 688. https://doi.org/10.1038/163688a0.

## STAR★METHODS

### KEY RESOURCES TABLE

| REAGENT or RESOURCE | SOURCE | IDENTIFIER |
|---|---|---|
| Antibodies | | |
| Ultra-LEAF™ Purified mouse anti-human CD3 (clone OKT3) | BioLegend | 317326; RRID: AB_11150592 |
| Mouse anti-human Akt (pS473) AF488 (clone M89-61) | BD Biosciences | 560404; RRID: AB_1645342 |
| Mouse anti-human CD1a FITC (clone HI149) | BioLegend | 300103; RRID: AB_314017 |
| Mouse anti-human CD2 PE (clone RPA-2.10) | BioLegend | 300207; RRID: AB_314031 |
| Mouse anti-human CD3 BUV395 (clone UCHT1) | BD Biosciences | 563546; RRID: AB_2744387 |
| Mouse anti-human CD3 APC-Cy7 (clone UCHT1) | BioLegend | 300426; RRID: AB_830755 |
| Mouse anti-human TCRαβ BV711 (clone IP26) | BioLegend | 306740; RRID: AB_2783169 |
| Mouse anti-human CD4 eF450 (clone RPA-T4) | Thermo Fisher Scientific | 48-0049-42; RRID: AB_1272057 |
| Mouse anti-human CD4 V500 (clone RPA-T4) | BD Biosciences | 560768; RRID: AB_1937323 |
| Mouse anti-human CD4 BB515 (clone SK3) | BD Biosciences | 565996; RRID: AB_2739447 |
| Mouse anti-human CD4 BV605 (clone RPA-T4) | BD Biosciences | 562658; RRID: AB_2744420 |
| Mouse anti-human CD4 BV786 (clone RPA-T4) | BD Biosciences | 740962; RRID: AB_2740587 |
| Mouse anti-human CD5 BV421 (clone UCHT2) | BD Biosciences | 562646; RRID: AB_2737700 |
| Mouse anti-human CD5 PE-Cy7 (clone UCHT2) | eBioscience | 25-0059-42; RRID: AB_1582282 |
| Mouse anti-human CD7 BV421 (clone M-T701) | BD Biosciences | 562635; RRID: AB_2736907 |
| Mouse anti-human CD7 BB515 (clone M-T701) | BD Biosciences | 565211; RRID: AB_2739113 |
| Mouse anti-human CD8α PE (clone SK1) | BioLegend | 980902; RRID: AB_2616623 |
| Mouse anti-human CD8α PE (clone HIT8α) | BD Biosciences | 555635; RRID: AB_395997 |
| Mouse anti-human CD8α BV605 (clone SK1) | BD Biosciences | 564116; RRID: AB_2869551 |
| Mouse anti-human CD8α BB700 (clone HIT8a) | BD Biosciences | 742229; RRID: AB_2740667 |
| Mouse anti-human CD8α BUV737 (clone RPA-T8) | BD Biosciences | 569189; RRID: AB_3099636 |
| Mouse anti-human CD8β PE-Cy7 (clone SIDI8BEE) | Thermo Fisher Scientific | 25-5273-42; RRID: AB_11219680 |
| Mouse anti-human CD8β BUV737 (clone 2ST8.5H7) | BD Biosciences | 748324; RRID: AB_2872743 |
| Mouse anti-human CD25 BB515 (clone 2A3) | BD Biosciences | 564467; RRID: AB_2744340 |
| Mouse anti-human CD25 PE (clone 4E3) | Miltenyi Biotec | 130-113-282; RRID: AB_2733790 |
| Mouse anti-human CD27 BV421 (clone M-T271) | BioLegend | 356418; RRID: AB_2562599 |

(*Continued on next page*)

*Continued*

| REAGENT or RESOURCE | SOURCE | IDENTIFIER |
|---|---|---|
| Mouse anti-human CD27 BB515 (clone M-T271) | BD Biosciences | 564642; RRID: AB_2744354 |
| Mouse anti-human CD27 PE-CF594 (clone M-T271) | BD Biosciences | 562297; RRID: AB_11154596 |
| Ultra-LEAF™ Purified mouse anti-human CD28 (clone CD28.2) | BioLegend | 302934; RRID: AB_11148949 |
| Mouse anti-human CD28 APC (clone CD28.2) | BioLegend | 302912; RRID: AB_314314 |
| Mouse anit-human CD28 PE-Cy5 (clone CD28.2) | BD Biosciences | 555730; RRID: AB_396073 |
| Mouse anti-human CD34 APC-Cy7 (clone 581) | BioLegend | 343514; RRID: AB_1877168 |
| Mouse anti-human CD40L APC (clone TRAP-1) | BD Biosciences | 555702; RRID: AB_398610 |
| Mouse anti-human CD43 PE (clone 1G10) | BD Biosciences | 560199; RRID: AB_1645655 |
| Mouse anti-human CD45 APC (clone HI30) | BD Biosciences | 555485; RRID: AB_398600 |
| Mouse anti-human CD45RO eF450 (clone UCHL1) | Thermo Fisher Scientific | 48-0457-42; RRID: AB_10852567 |
| Mouse anti-human CD45RA PE-Cy7 (clone HI100) | Thermo Fisher Scientific | 25-0458-42; RRID: AB_1548774 |
| Mouse anti-human CD45RA BV605 (clone HI100) | BD Biosciences | 562886; RRID: AB_2737865 |
| Mouse anti-human CD45RA BV785 (clone HI100) | BioLegend | 304140; RRID: AB_2563816 |
| Mouse anti-human CD56 BUV563 (clone NCAM16.2) | BD Biosciences | 612929; RRID: AB_2916880 |
| Mouse anti-human CD62L PE (clone DREG-56) | BD Biosciences | 555544; RRID: AB_395928 |
| Mouse anti-human CD62L PE-Cy5 (clone DREG-56) | BD Biosciences | 555545; RRID: AB_395929 |
| Mouse anti-human CD62L PerCP-eF710 (clone DREG-56) | Thermo Fisher Scientific | 46-0629-42; RRID: AB_1834409 |
| Mouse anti-human CD69 APC (clone FN50) | BioLegend | 310910; RRID: AB_314845 |
| Mouse anti-human CD69 PE-Cy5 (clone FN50) | BioLegend | 310908; RRID: AB_314843 |
| Mouse anti-human CD69 BV786 (clone FN50) | BD Biosciences | 563834; RRID: AB_2738441 |
| Mouse anti-human CD71 BV786 (clone M-A712) | BD Biosciences | 563768; RRID: AB_2738414 |
| Mouse anti-human CD127 PE-CF594 (clone HIL 7R M21) | BD Biosciences | 562397; RRID: AB_11154212 |
| Mouse anti-human CD127 APC-AF700 (clone R34.34) | Beckman Coulter | A71116; RRID: AB_2889979 |
| Mouse anti-human CD134 (OX40) PE (clone ACT35) | BD Biosciences | 561700; RRID: AB_10893600 |
| Mouse anti-human CD137 (4-1BB) PE-Cy7 (clone 4B4-1) | BioLegend | 309818; RRID: AB_2207741 |
| Mouse anti-human CCR4 PE/Dazzle594 (clone L291H4) | BioLegend | 359420; RRID: AB_2564095 |
| Mouse anti-human CCR6 BV605 (clone G034E3) | BioLegend | 353420; RRID: AB_2561449 |
| Mouse anti-human CCR6 BV785 (clone G034E3) | BioLegend | 353422; RRID: AB_2563660 |

(*Continued on next page*)

*Continued*

| REAGENT or RESOURCE | SOURCE | IDENTIFIER |
|---|---|---|
| Mouse anti-human CCR7 BV605 (clone 2-L1-A) | BD Biosciences | 566754; RRID: AB_2869850 |
| Mouse anti-human CCR7 BUV661 (clone 2-L1-A) | BD Biosciences | 749824; RRID: AB_2874072 |
| Mouse anti-human CXCR3 BV421 (clone G025H7) | BioLegend | 353716; RRID: AB_2561448 |
| Mouse anti-human CXCR3 PE (clone G025H7) | BioLegend | 353706; RRID: AB_10962912 |
| Mouse anti-human Erk1/2 (pT202/pY204) BV421 (clone 20A) | BD Biosciences | 562981; RRID: AB_2737930 |
| Mouse anti-human GATA-3 PE-Cy7 (clone L50-823) | BD Biosciences | 560405; RRID: AB_1645544 |
| Mouse anti-human IFNγ FITC (clone B27) | BD Biosciences | 552887; RRID: AB_394516 |
| Mouse anti-human IFNγ Purified (clone B27) | BD Biosciences | 554698; RRID: AB_395516 |
| Mouse anti-human IL-2 BV421 (clone MQ1-17H12) | BD Biosciences | 564164; RRID: AB_2738635 |
| Mouse anti-human IL-4 Purified (clone MP4-25D2) | BD Biosciences | 554481; RRID: AB_395421 |
| Mouse anti-human IL-4 BV711 (clone MP4-25D2) | BD Biosciences | 564112; RRID: AB_2738600 |
| Mouse anti-human IL-17A BV786 (clone N49-653) | BD Biosciences | 563745; RRID: AB_2738401 |
| Mouse anti-human IL-17F BV786 (clone O33-782) | BD Biosciences | 564265; RRID: AB_2869556 |
| Mouse anti-human NF-kB (pS529) PE (clone K10-859.12.50) | BD Biosciences | 558423; RRID: AB_647222 |
| Mouse anti-human NFATc3 (pS240) AF647 (clone C-3) | Santa Cruz Biotechnology | sc-365786 AF647; RRID: AB_10844623 |
| Mouse anti-human RORγt BV421 (clone Q21-559) | BD Biosciences | 563282; RRID: AB_2738114 |
| Mouse anti-human RORγt PE (clone Q21-559) | BD Biosciences | 563081; RRID: AB_2686896 |
| Mouse anti-human RUNX3 BV421 (clone R3-5G4) | BD Biosciences | 565742; RRID: AB_2916369 |
| Mouse anti-human SSEA4 APC (clone MC-813-70) | BioLegend | 330417; RRID: AB_2616818 |
| Mouse anti-human T-bet AF647 (clone 4-B10) | BD Biosciences | 561264; RRID: AB_10563424 |
| Mouse anti-human ThPOK PE (clone 11H11A14) | BioLegend | 656404; RRID: AB_2563009 |
| Mouse anti-human TRA-1-81 PE (clone TRA-1-81) | BioLegend | 330708; RRID: AB_1089243 |
| Mouse anti-human ZAP70 (pY319) / Syk (pY352) PE-Cy7 (clone 17A/P-ZAP70) | BD Biosciences | 561458; RRID: AB_10696417 |
| TotalSeq™-C Human Universal Cocktail, V1.0 | BioLegend | 399905; RRID: AB_2876728 |
| **Biological samples** | | |
| Human postnatal thymus from thymectomy (Donor ID: sex, age): T085: M, 8 months old | BC Children's Hospital | N/A |
| Human postnatal thymus from thymectomy (Donor ID: sex, age): T087: F, 4 months old | BC Children's Hospital | N/A |
| Human postnatal thymus from thymectomy (Donor ID: sex, age): T088: M, 4.5 months old | BC Children's Hospital | N/A |

(*Continued on next page*)

*Continued*

| REAGENT or RESOURCE | SOURCE | IDENTIFIER |
|---|---|---|
| Human postnatal thymus from thymectomy (Donor ID: sex, age): T100: M, 4 months old | BC Children's Hospital | N/A |
| Human postnatal thymus from thymectomy (Donor ID: sex, age): T110: M: 7 weeks old | BC Children's Hospital | N/A |
| Human postnatal thymus from thymectomy (Donor ID: sex, age): T116: F, 3 months old | BC Children's Hospital | N/A |
| Human postnatal thymus from thymectomy (Donor ID: sex, age): T120: M, 12 months old | BC Children's Hospital | N/A |
| Human postnatal thymus from thymectomy (Donor ID: sex, age): T121: M, 3.8 months old | BC Children's Hospital | N/A |
| Human postnatal thymuses from thymectomies (Donor ID: sex, age): T133: F, 6 months old | BC Children's Hospital | N/A |
| Buffy coat from healthy adult (Donor ID: sex, age): C5621: F, 47 years old | Canadian Blood Services | https://www.blood.ca/en |
| Buffy coat from healthy adult (Donor ID: sex, age): C5851: M, 33 years old | Canadian Blood Services | https://www.blood.ca/en |
| Buffy coat from healthy adult (Donor ID: sex, age): C5853: M, 35 years old | Canadian Blood Services | https://www.blood.ca/en |
| Buffy coat from healthy adult (Donor ID: sex, age): C5859: F, 29 years old | Canadian Blood Services | https://www.blood.ca/en |
| **Chemicals, peptides, and recombinant proteins** | | |
| Ammonium Chloride Solution | STEMCELL Technologies | 07850 |
| L-Ascorbic acid 2-phosphate sesquimagnesium salt hydrate | Sigma-Aldrich | A8960 |
| B-27™ Supplement (50X), minus vitamin A | Life Technologies | 12587010 |
| Brilliant Stain Buffer Plus | BD Biosciences | 566385 |
| CHIR 99021 | Tocris Bioscience | 4423 |
| Cytofix™ Fixation Buffer | BD Biosciences | 554655 |
| DNase I recombinant, RNase-free | Sigma Aldrich | 04716728001 |
| DNase I Solution (1 mg/mL) | STEMCELL Technologies | 07900 |
| eBioscience™ Cell Proliferation Dye eFluor™ 450 | Thermo Fisher Scientific | 65-0842-85 |
| eBioscience™ Fixable Viability Dye eFluor™ 780 | Thermo Fisher Scientific | 65-0865-18 |
| GlutaMAX™ Supplement | Thermo Fisher Scientific | 35050061 |
| Ionomycin calcium salt | Sigma-Aldrich | I0634 |
| Penicillin-Streptomycin (10,000 U/mL) | GIBCO | 15140163 |
| Phorbol 12-myristate 13-acetate (PMA) | Sigma Aldrich | P8139 |
| Phytohemagglutinin-L (PHA-L) | Sigma Aldrich | 11249738001 |
| Phytohemagglutinin (PHA-M) | ChemScene | CS-0101581 |
| Recombinant Human BMP-4 Protein | R&D Systems | 314-BP-050 |
| Recombinant Human/Rhesus Macaque/ Feline CXCL12/SDF-1 alpha | R&D Systems | 350-NS |
| Recombinant Human DLL1 Fc Chimera Protein, CF | R&D Systems | 10184-DL |
| Recombinant Human DLL4 Protein (ECD, hFc Tag), HPLC-verified | Sino Biologicals | 10171-H02H |
| Recombinant Human EPO (Erythropoietin) Protein | Thermo Fisher Scientific | 100-64 |
| Recombinant Human FGF-basic (FGF-2/bFGF) (154 aa) Protein | Thermo Fisher Scientific | 100-18B |

(*Continued on next page*)

*Continued*

| REAGENT or RESOURCE | SOURCE | IDENTIFIER |
|---|---|---|
| Recombinant Human Flt-3 Ligand/FLT3L Protein | R&D Systems | 308-FK |
| Recombinant Human IGF-I/IGF-1 Protein, CF | R&D Systems | 291-G1 |
| Recombinant Human IL-1β | STEMCELL Technologies | 78034.1 |
| Recombinant Human IL-2 (Proleukin) | Iovance Biotherapeutics | 02130181 |
| Recombinant Human IL-2 Protein | STEMCELL Technologies | 78036 |
| Recombinant Human IL-3 Protein | R&D Systems | 203-IL |
| Recombinant Human IL-4 Protein | STEMCELL Technologies | 78045 |
| Recombinant Human IL-6 Protein | STEMCELL Technologies | 78148 |
| Recombinant Human IL-6 Protein | R&D Systems | 206-IL |
| Recombinant Human IL-7 Protein | R&D Systems | 207-IL |
| Recombinant Human IL-11 Protein | R&D Systems | 218-IL |
| Recombinant Human IL-12 (p70) | BD Biosciences | 554613 |
| Recombinant Human IL-15 Protein | R&D Systems | 247-ILB |
| Recombinant Human IL-18 Protein | R&D Systems | 9124-IL |
| Recombinant Human IL-21 Protein | R&D Systems | 8879-IL |
| Recombinant Human IL-23 Protein | Thermo Fisher Scientific | 200-23-10UG |
| Recombinant Human Jagged 1 Fc Chimera Protein, CF | R&D Systems | 1277-JG |
| Recombinant Human Jagged 2 Fc Chimera Protein, CF | R&D Systems | 1726-JG |
| Recombinant Human SCF Protein | R&D Systems | 255-SC |
| Recombinant Human TGF-beta 1 (CHO-Expressed) Protein, CF | R&D Systems | 11409-BH-010 |
| Recombinant Human Thrombopoietin (TPO, NS0-expressed) Protein | R&D Systems | 288-TPN |
| Recombinant Human TNF-alpha Protein | R&D Systems | 210-TA |
| Recombinant Human VEGF 165 Protein | R&D Systems | 293-VE |
| Recombinant Mouse VCAM-1/CD106 Fc Chimera Protein, CF | R&D Systems | 643-VM-200 |
| RetroNectin | Takara Bio (Cedarlane) | T100B(CB) |
| ROCK Inhibitor Y-27632 | STEMCELL Technologies | 72308 |
| SB 431542 hydrate | Sigma-Aldrich | S4317 |
| Transferrin | Sigma-Aldrich | 10652202001 |
| Z-VAD-FMK | R&D Systems | FMK001 |
| Zombie UV™ Fixable Viability Kit | BioLegend | 423108 |
| 1-Thioglycerol | Sigma-Aldrich | M6145 |
| 2-Mercaptoethanol | Sigma-Aldrich | M3148 |
| **Critical commercial assays** | | |
| Absolutely RNA Nanoprep Kit | Agilent | 400753 |
| CD34 MicroBead Kit, human | Miltenyi Biotec | 130-046-702 |
| Cytofix/Cytoperm™ Fixation/ Permeabilization Kit | BD Biosciences | 554714 |
| EasySep™ Human Naïve $CD4^+$ T Cell Isolation Kit | STEMCELL Technologies | 19555 |
| EasySep™ Release Human CD3 Positive Selection Kit | STEMCELL Technologies | 17751 |
| eBiosciences FoxP3 / Transcription Factor Staining Buffer Set | Thermo Fisher Scientific | 00-5523-00 |
| RosetteSep Human $CD4^+$ T Cell Enrichment Cocktail | STEMCELL Technologies | 15062 |

(*Continued on next page*)

*Continued*

| REAGENT or RESOURCE | SOURCE | IDENTIFIER |
|---|---|---|
| **Deposited data** | | |
| CITE-seq iPS11-derived T cells at Maturation Day M14 in PSC2 media | This Study | Mendeley Data: https://doi.org/10.17632/k3xtwnzpyn.1 |
| CITE-seq + scTCR-seq iPS11-derived T cells at Expansion Day X11 in PSC4 media | This Study | Same as above |
| Analysis code and generated outputs for Day M14 CITE-seq data | This Study | GitHub: https://github.com/stemcellbioengineering/stankiewicz-michaels-M14; Zenodo: https://doi.org/10.5281/zenodo.17861714 |
| Analysis code and generated outputs for Day X11 CITE-seq and scTCRseq data | This Study | GitHub: https://github.com/stemcellbioengineering/jones-salim-cd4; Zenodo: https://doi.org/10.5281/zenodo.17861549 |
| **Experimental models: Cell lines** | | |
| iPS11 human iPSC line (Episomal, HFF-derived) | ALSTEM | iPS11; RRID: CVCL_E7BE |
| H1 human ESC line | WiCell | WA01; RRID: CVCL_9771 |
| **Oligonucleotides** | | |
| See Table S6 | Shukla et al.[97]; Jia et al.[98]; De Decker et al.[99]; Karthaus et al.[100] | N/A |
| **Software and algorithms** | | |
| CytExpert v2.6 | Beckman Coulter | https://www.beckman.com/flow-cytometry/research-flow-cytometers/cytoflex/software |
| FlowJo v10.8.2 | BD Biosciences | https://www.flowjo.com/solutions/flowjo |
| ImageJ | NIH | https://imagej.net/ij/ |
| Prism v10 | GraphPad | https://www.graphpad.com/features |
| Anaconda Python 3 Core | Anaconda | https://anaconda.org/anaconda/python |
| CRISP | Wang et al.[101] | https://github.com/will-yx/ |
| HFcluster | Wang et al.[101] | https://github.com/will-yx/ |
| Scanpy 1.10.4 | Wolf et al.[102] | https://github.com/scverse/scanpy |
| ThresholdPy 0.1.5 | Adapted from ThresholdR (Oliaeimotlagh et al.[68]) | https://github.com/jonesr18/ThresholdPy |
| FlowKit 1.2.3 | White et al.[103] | https://github.com/whitews/flowkit |
| Scirpy 0.22.3 | Sturm et al.[104] | https://github.com/scverse/scirpy |
| **Other** | | |
| AggreWell™400 | STEMCELL Technologies | 34425 |
| Anti-Adherence Rinsing Solution | STEMCELL Technologies | 07010 |
| ArC™ Amine Reactive Compensation Bead Kit | Thermo Fisher Scientific | A10346 |
| BD Pharmingen™ Human BD Fc Block™ | BD Biosciences | 564220 |
| Belzer UW Cold Storage Solution | Bridge to Life | BUW-001 |
| Bovine Serum Albumin (BSA, Sterile 20%) | Wisent Bioproducts | 809-098-EL |
| CellDrop Cell Counter | DeNovix | N/A |
| Cellometer Spectrum Cell Counter | Revvity | N/A |
| CryoStor® CS10 | STEMCELL Technologies | 07930 |
| Cultrex Stem Cell Qualified Reduced Growth Factor Basement Membrane Extract | Bio-techne | 3434-010-02 |
| FACSAria™ Fusion Cell Sorter | BD Biosciences | N/A |
| Fetal Bovine Serum, qualified, Canada | GIBCO | 12483020 |

(*Continued on next page*)

*Continued*

| REAGENT or RESOURCE | SOURCE | IDENTIFIER |
|---|---|---|
| Foxp3/Transcription Factor Staining Buffer Set | Thermo Fisher Scientific | 00-5523-00 |
| Fc Receptor Binding Inhibitor Polyclonal Antibody | Thermo Fisher Scientific | 14-9161-73 |
| Geltrex™ hESC-Qualified, Ready-To-Use, Reduced Growth Factor Basement Membrane Matrix | GIBCO | A1569601 |
| GentleMACS Tissue Dissociator | Miltenyi Biotec | N/A |
| HBSS, no calcium, no magnesium, no phenol red | GIBCO | 14175103 |
| ImmunoCult™ Human CD3/CD28/CD2 T Cell Activator | STEMCELL Technologies | 10970 |
| ImmunoCult™ Human CD3/CD28 T Cell Activator | STEMCELL Technologies | 10971 |
| ImmunoCult™-XF T Cell Expansion Medium | STEMCELL Technologies | 10981 |
| Lymphoprep™ | STEMCELL Technologies | 07861 |
| PowerUp SYBR Green Master Mix | Applied Biosystems | A25742 |
| MoFlo Astrios Cell Sorter | Beckman Coulter | N/A |
| mTeSR™1 | STEMCELL Technologies | 85850 |
| mTeSR™ Plus | STEMCELL Technologies | 100-0276 |
| OneComp eBeads™ Compensation Beads | Thermo Fisher Scientific | 01-1111-42 |
| RPMI 1640 Medium | GIBCO | 11875093 |
| PBS, pH7.4 (1x) | Thermo Fisher | 10010049 |
| PhenoCycler (CODEX) | Akoya Biosciences | N/A |
| SD100 Counting Chambers | Revvity | CHT4-SD100 |
| StemPro™-34 SFM (1X) | Thermo Fisher Scientific | 10639011 |
| StemSpan™ T Cell Progenitor Maturation Supplement (10X) | STEMCELL Technologies | 09930 |
| StemSpan™ SFEM II | STEMCELL Technologies | 09655 |
| Superscript IV VILO Master Mix | Invitrogen | 11-756-050 |
| Trypan Blue | Thermo Fisher Scientific | 15250061 |
| TrypLE™ Express Enzyme (1X), phenol red | GIBCO | 12605028 |
| Ultra Rainbow Calibration Particles, 6 peaks | Spherotech | URCP-38-2K |
| VersaComp Antibody Capture Beads | Beckman Coulter | B22804 |
| ViaStain™ AOPI Staining Solution | Revvity | CS2-0106 |

## EXPERIMENTAL MODEL AND STUDY PARTICIPANT DETAILS

Sex was not considered as a variable in this study. Though sex is known to affect T cell development *in vivo*,[37] it is unknown if any such effects translate to *in vitro* cultures.

### Human pluripotent stem cell (hPSC) lines

iPS11 cells (male, human foreskin fibroblast episomal-derived iPSCs) were acquired from ALSTEM (iPS11). H1 cells[105] (male, human embryonic stem cells) were acquired from WiCell (WA01). Both cell types were maintained in mTeSR™1 or mTeSR™ Plus media (STEMCELL Technologies) supplemented with 0.5% penicillin/streptomycin (GIBCO) and in normoxic conditions (20% $O_2$, 37°C, 5% $CO_2$). Cells were grown on tissue culture-treated plastic plates coated for 1 hour at 37°C with Geltrex (GIBCO) or Cultrex (Bio-Techne). For passaging and seeding HE differentiations, PSCs were dissociated to small clusters by incubating in TrypLE Express (GIBCO) for 2-4 min at 37°C, followed by quenching with mTeSR™1 or mTeSR™ Plus and light pipetting. On thaw or passage, cells were treated with 5 μM ROCK inhibitor (ROCKi) Y-27632 (STEMCELL Technologies).

### Patient samples

Human research was approved by the University of British Columbia Research Ethics Board (H17-01490 and H18-02553). All samples used for this study were obtained with written informed consent from parents/guardians of participants (for thymus samples) and

participants (for buffy coats). Donor sex and age for each thymus or buffy coat donor can be found in "key resources table." Thymus donors were screened for prior to sample collection and excluded from this study if known developmental and genetic disorders were present. Buffy coat samples were screened for infectious diseases and excluded from study if they are tested positive. Ancestry, gender, ethnicity, and socioeconomic status were not collected as part of this study.

## METHOD DETAILS

### CODEX image analysis of Notch ligand density in postnatal thymus

Postnatal thymus images were previously acquired via Co-detection by indexing (CODEX) imaging.[37] Three representative images which captured a full thymus lobule (i.e. Capsule, cortex, and full medulla) from donor T085 (M, 8 mo) were chosen for analysis of Notch ligands. For each image, ImageJ was used to draw three lines of thickness 10 from the center of the medulla to the outer edge of the cortex, with the center of the line overlaying the corticomedullary junction. Signal intensity was recorded along the length of the line and binned into 20 segments. The average signal intensity was calculated for each bin. Signal intensities from each line were averaged for each ligand and plotted with GraphPad Prism (v10, GraphPad Software).

### PSC to HE differentiation

Differentiations of PSCs to $CD34^+$ HE cells followed our published AggreWell-based protocol[13] with minor modifications. All media formulations are provided in Table S7. AggreWell 400 6-well plates (STEMCELL Technologies) were prepared by coating with 2 mL Anti-Adherence Rinsing Solution (STEMCELL Technologies), spinning down for 5-10 min at 1300 x g (to remove bubbles), incubating for 2 hours at room temperature, then washing with 2 mL PBS. PSCs were grown to 50-75% confluency, then dissociated to single cells by incubating in TrypLE Express for 3-5 min at 37°C, followed by quenching with mTeSR1 or mTeSR Plus and moderate pipetting. Collected cells were spun down at 200 g for 5 min, then resuspended to 2.21 million cells/mL in "T0" media. T0 media comprises 0.0039% 1-thioglycerol (MTG) (Sigma-Aldrich), 50 μg/mL ascorbic acid (AA) (Sigma-Aldrich), 150 μg/mL Transferrin (Sigma-Aldrich), 10 ng/mL BMP4 (R&D Systems), and 5 μM ROCKi Y-27632 supplemented into StemPro "Complete" base media. StemPro Complete comprises StemPro 34 (Thermo Fisher Scientific) supplemented with 1% GlutaMax (Thermo Fisher) and 0.5% Pen/Strep. Aiming for 75 cells/microwell, we added 2 mL T0-cell suspension per 6-well of the AggreWell plate. To achieve uniform aggregation, we allowed cells to evenly settle at RT for 5 minutes, then spun down for 5 min at 200 x g. Throughout the HE induction, cells were grown in hypoxic conditions (5% $O_2$, 37°C, 5% $CO_2$).

Differentiating cells were subsequently fed at 24, 42, 72, 96, and 144 hours with "T1", "T1.75", "T3", "T4", and "T6" media, respectively. The T1, T3, and T6 feeds were each 2 mL media top-ups, while T1.75 and T4 feeds involved carefully aspirating the existing media and adding 2 mL fresh media. Media aspirations and additions were done slowly and at the same edge of each well to minimize disturbances to the aggregates. Each media formulation uses StemPro compete as base and contains the same concentrations of MTG, AA, and Transferrin as in T0 media. T1 media further contains 10 ng/mL BMP4 and 10* ng/mL bFGF (Thermo Fisher) [*the latter achieving a final concentration of 5 ng/mL after topping-up the existing T0 media in each well]. T1.75 and T3 media (equivalent) further contain 10 ng/mL BMP4, 5 ng/mL bFGF, 6 μM SB-431542 (Sigma-Aldrich), and 4 μM CHIR-99021 (Tocris Bioscience). T4 media further contains 5 ng/mL bFGF, 15 ng/mL VEGF (R&D Systems), 10 ng/mL IL6 (R&D Systems), and 5 ng/mL IL11 (R&D Systems). T6 media contains the same factors as T4 media along with 50* ng/mL SCF (R&D Systems), 4* U/mL EPO (Thermo Fisher), and 50* ng/mL IGF-1 (R&D Systems) [*each achieving half the stated concentrations after topping-up the existing T4 media in each well].

$CD34^+$ HE cells were collected 192 hours (day 8, "T8") after initiation of differentiation. Aggregates were collected, spun down at 200 g for 5 min, then dissociated to single cells by incubating in 0.5 mL (per pooled 6-well) TrypLE supplemented with 100 U/mL DNase I (Sigma-Aldrich) for 15 min at 37°C, vigorously pipetting every 5 min. The TrypLE was quenched with a 50:50 mix of HBSS (GIBCO) and FBS (GIBCO). Cells were spun down for 5 min at 200 x g, washed in 3 mL HBSS +2% FBS, then resuspended in 1 mL HBSS +2% FBS for pre-enrichment counting; a subset of cells was set aside for flow cytometry. $CD34^+$ cells were isolated using the human CD34-MicroBead kit (Miltenyi Biotec), as per the manufacturer's instructions. Post-enrichment cells were counted and frozen down in CryoStor CS10 (STEMCELL Technologies) at 1 million cells/mL; a subset of cells was set aside for flow cytometry. The set-aside pre- and post-enrichment cells were stained with antibodies against key markers: CD34, CD43, CD73, and CD184 to validate HE induction.[106]

### PSC-HE to DP T cell differentiation

PSC-T cell differentiations generally followed our published protocol,[13] with minor modifications. All media formulations are provided in Table S7. In all cases, cells were incubated in normoxic conditions (20% $O_2$, 37°C, 5% $CO_2$). For PSC-HE to HSPC induction, wells were prepared by coating TC-treated plates with 10-15 (typically 15) μg/mL hDLL4-Fc (Sino Biological) + 2.5 μg/mL mVCAM1 (R&D Systems) for 2 hours at RT or 37°C, or overnight at 4°C. PSC-HE cells were thawed and seeded at 30-100 (typically 100) x $10^3$ cells/mL (3-10 x $10^3$ cells/100 μL per 96-well) in EHT media. EHT media contains the same factors as T4 media (see above) with VEGF reduced to 5 ng/mL and additionally supplemented with 10 ng/mL BMP4, 50 ng/mL SCF, 30 ng/mL TPO (R&D Systems), 25 ng/mL IGF-1, 10 ng/mL IL3 (R&D Systems), 10 ng/mL Flt3L (R&D Systems), and 10 μM ROCKi Y-27632. Cells were collected via light pipetting and passaged to Pro-T induction conditions at EHT day 4-7 (annotated E4-7; typically E5).

For PSC-HSPC to Pro-T induction, wells were prepared by coating with 10-15 (typically 15) μg/mL hDLL4-Fc + 2.5 μg/mL mVCAM1 for 2 hours at RT or 37°C, or overnight at 4°C. Cells output from the HSPC induction stage were seeded at 30-100 (typically 100) x $10^3$ cells/mL (3-10 x $10^3$ cells/100 μL per 96-well) in "PSC1" media. PSC1 comprises 12.37 ng/mL SCF, 8.61 ng/mL Flt3L, 97.4 ng/mL CXCL12 (R&D Systems), 0.07 ng/mL TNFα (R&D Systems), 0.97 ng/mL IL3, and 65.25 ng/mL IL7 (R&D Systems) supplemented into "JAC Ultra" base media. JAC Ultra comprises IMDM with GlutaMAX (GIBCO) supplemented with 4% B27 without Vitamin A (Thermo Fisher), 0.5% Pen/Strep, 24 μM BME (Sigma-Aldrich) and 60 μM AA. Cells were fed by top-up with an equal volume of fresh media at Pro-T induction day 3 or 4 (annotated P3 or P4). Cells were sampled for flow cytometry and passaged to DP induction conditions between day P7-9 (typically P7).

For iPSC-Pro-T to DP maturation, wells were prepared by coating with 10-15 (typically 10) μg/mL hDLL4-Fc + 2.5 μg/mL mVCAM1 for 2 hours at RT or 37°C, or overnight at 4°C. Cells output from the Pro-T induction stage were seeded at 0.5-4 (typically 2) x $10^6$ cells/mL (50-400 x $10^3$ cells/100 μL per 96-well) in "PSC2" media (Figures 1, 2, 5, 6, S1, S2A–S2D, S3A, S3B, and S6). PSC2 comprises 9.76 ng/mL SCF, 4.96 ng/mL Flt3L, 15.22 ng/mL CXCL12/SDF-1, 0.04 ng/mL TNFα, 2.55 ng/mL IL3, and 71.93 ng/mL IL7 supplemented into "JAC Ultra" base media. Where indicated, cells were instead seeded into media comprising StemSpan T cell Progenitor Maturation Supplement (STEMCELL Technologies) diluted 1:10 into either JAC Ultra (Figures 3, S2, S3C, and S5) or SFEM II (STEMCELL Technologies) (Figures 4, 7, S2A–S2G, S4, and S7). Cells were fed by top-up with an equal volume of fresh media at DP maturation day 3 or 4 (annotated M3 or M4). Thereafter, cells were fed by 50% media exchange with an equal volume of fresh media every 3-4 days. Cells were typically sampled for flow cytometry every ~7 days (e.g. days M7, M14, and M21). Cells were induced to SP cells starting between day M14-28 (typically M21), aiming for the population of $CD3^+TCR\alpha\beta^+$ cells to be >10% among live cells.

### PSC-DP to SP T cell differentiation

General protocol: for iPSC-DP to SP induction, wells were prepared by coating with 0-10 μg/mL hDLL4-Fc, hDLL1-Fc (R&D Systems), hJAG1-Fc (R&D Systems), or hJAG2-Fc (R&D Systems) + 2.5 ug/mL mVCAM-1 for 2 hours at RT or 37°C, or overnight at 4°C. Where indicated, the wells were left uncoated. Cells output from the DP induction stage were seeded 1:1 in the same media in which they were matured to DPs, supplemented with 0-2.5% Immunocult anti-CD2/3/28 complexes (Figures 1, 2, 3, 4, 5, S1, S2, S3, S4, S5, and S6; STEMCELL Technologies), 0-2.5 μg/mL PHA-M (Figures 2 and S3; ChemScene) or PMA-L (Figures 3 and S4; Sigma-Aldrich), or 0-0.25 ng/mL PMA (Figures 2 and S3; Sigma-Aldrich) + 100 ng/mL Ionomycin (Sigma-Aldrich). SP induction periods lasted 7-14 days. Cells were fed by top-up with an equal volume of fresh media (without stimulating reagents) at SP induction day 3 or 4 (annotated S3 or S4). For 14 day stimulations, on S7 cells were either passaged 1:1 onto uncoated wells or wells freshly coated with 2.5 μg/mL mVCAM1 only, or fed by 50% media exchange, both with fresh media without stimulation, as indicated in figure legends. In both cases, cells were fed again with fresh media (without stimulation) at day S10 or S11. Cells were typically sampled for flow cytometry on days S7 and S14. In some cases, cells were sampled for flow cytometry or RT-qPCR at earlier timepoints (e.g. 24-72 hours after stimulation). Where indicated, cells were transferred to expansion conditions after 7-14 days SP induction.

SP induction details per figure: Figure 1C: iPSC-derived cells matured towards DPs in PSC2 media for 2-3 weeks were re-seeded into wells coated with 10-15 μg/mL DLL4 + 2.5 μg/mL VCAM1 and in PSC2 media supplemented with anti-CD2/3/28 to induce positive selection to SP cells. Cells were fed three days later without additional TCR stimulation, then measured on day S7. Figures 1E and 1F: iPSC-derived cells matured towards DPs for 3 weeks in PSC2 media were re-seeded into wells coated with 10 μg/mL Notch ligand +2.5 μg/mL VCAM1 and in PSC2 media supplemented with 0.1% anti-CD2/3/28 (added only during initial seeding, not later feeds) and 0-10 μM DAPT (added during all subsequent feeds), then measured on day S14. Figures 1G and 1H: iPSC-derived cells matured as in (Figure 1E), then seeded into wells coated with 2.5 μg/mL VCAM-1 ± 10 μg/mL different Notch ligands in PSC2 media supplemented with 0.1% anti-CD2/3/28 ± 5 μM DAPT, and measured on day S14. Figure 2: iPSC-derived cells matured towards DPs in PSC2 media for 3 weeks were re-seeded into wells freshly coated with different levels of DLL4 + 2.5 μg/mL VCAM1 and in PSC2 media supplemented with different levels of TCR pathway activators (anti-CD2/3/28, PHA-M, PMA+Iono) to induce positive selection to SP cells. Cells were fed three days later without additional TCR stimulation, then rested for a week by passaging onto wells coated with VCAM1 only and in PCS2 media without TCR stimulation, and finally measured on day S14. Figures 3A–3E: iPSC-derived cells were matured towards DPs for 2 weeks in SCT SFEM media, then transferred into different downstream conditions: DP-skewing: 15 μg/mL DLL4 and no stimulation; 4SP-skewing: 0 μg/mL DLL4 and stimulation with 0.1% anti-CD2/3/28 or 0.5 μg/mL PHA-L; or 8SP-skewing: 15 μg/mL DLL4 and stimulation with 0.1% anti-CD2/3/28 or 0.5 μg/mL PHA-L; all in SCT SFEM media. Expression of relevant markers were measured on day S7 (panels B-E) and S14 (panel E). Figures 3F and 3G: see below. Figure 4: iPSC-derived cells were matured towards DPs in SCT JAC media for 3 weeks, then re-seeded into SCT JAC media supplemented with 0.3% vs 1.25% anti-CD2/3/28 ± 5 μM DAPT on wells coated with 2.5 μg/mL VCAM1 ± DLL4. Cells were sampled at the indicated times for staining intracellular TFs + surface markers or intracellular phosphorylated proteins. Figures 5 and 6: iPSC-derived cells at two weeks of DP maturation were induced to SP cells over two weeks in conditions with approximately equal bias (0.1% [week 1], then 0.3% [week 2] anti-CD2/3/28, on 10 μg/mL DLL4 + 2.5 μg/mL VCAM1 [both weeks]). $CD3^+$ cells were then magnetically enriched, rested for one week, and expanded on CD3 [clone OKT3] + RetroNectin in IL-7/IL-15-based media (see below for additional details). Figure 7: see below.

Details for SP inductions in supplementary figures are included in their captions.

### PSC-CD4$^+$ T cell generation and isolation for expansion and polarization tests

For cells used in Figures 3F, 3G, 7, S4, and S7, iPSC-HE to HSPC induction and iPSC-HSPC to Pro-T induction were carried out as above. For iPSC-Pro-T to DP maturation, wells were prepared by coating with 15 μg/mL hDLL4 + 2.5 μg/mL mVCAM1. iPSC-Pro-T cells were seeded at 3 x $10^6$ cells/mL (300 x $10^3$ cells/100 μL per 96-well) in StemSpan media. (StemSpan T cell Progenitor Maturation Supplement diluted 1:10 into SFEM II; STEMCELL Technologies). Cells were fed by top-up with an equal volume of fresh StemSpan media at DP maturation day M3 or M4, then fed by 50% media exchanges every 3-4 days until day M14. For iPSC-DP to 4SP induction, day M14 cells were collected, centrifuged, resuspended in StemSpan media supplemented with 0.5 μg/mL PHA-L for stimulation, and plated into uncoated 6-well plates (9 x $10^3$ cells/5mL per 6-well). Cells were fed by 50% media exchange with an equal volume of fresh StemSpan media (without stimulation) 3-4 days post-stimulation (S3-4). On days S7 and S10, cells were fed by 50% media exchange with Immunocult-XF T Cell Expansion Media (STEMCELL Technologies) supplemented with 200 IU/mL IL-2 (Proleukin). On day S14, cells were collected, stained for antibodies for 15 min at room temperature, and sorted for iPSC-CD4$^+$ T cells (TCRαβ$^+$CD4$^+$CD8α$^-$) using MoFlo Astrios (Beckman Coulter) or FACSAria Fusion (BD Biosciences). Flow-sorted cells were subsequently used for experiments.

### CD4$^+$ T cell isolation from human postnatal thymus

Following informed consent, human postnatal thymus tissue was collected in UW Solution (Bridge to Life) from neonates (donor sex and age can be found in "key resources table") undergoing cardiac surgeries in BC Children's Hospital. Approximately 3 g piece of the thymus tissue was mechanically dissociated in Immunocult-XF T cell Expansion Medium using GentleMACS Dissociator (Miltenyi Biotec). The dissociated bulk thymocytes were filtered and subsequently frozen for further use. On day of experiment, frozen bulk thymocytes were thawed, treated with DNAseI (1 mg/mL final concentration; STEMCELL Technologies) for 10 min at room temperature, stained with antibodies at 15 min at room temperature, and flow-sorted for thymic-CD4$^+$ T cells (TCRαβ$^+$CD25$^-$CD4$^+$CD8α$^-$) using FACSAria Fusion (BD Biosciences). Flow-sorted cells were subsequently used for experiments.

### CD4$^+$ T cell isolation from human adult peripheral blood

Buffy coats (Canadian Blood Services) were obtained from consented healthy adult donors and enriched for CD4$^+$ cells prior to flow sorting (donor sex and age can be found in "key resources table"). Blood samples were incubated with RosetteSep Human CD4$^+$ T Cell Enrichment (STEMCELL Technologies) at room temperature for 20 minutes, diluted in 1:1 ratio with 1X PBS (GIBCO), layered atop Lymphoprep (15 mL/tube, STEMCELL Technologies), and fractionated by centrifugation (582 x g, 25 min, no brake, room temperature). The buffy coat layer was collected using transfer pipettes, and red blood cells within the layer were lysed using Ammonium Chloride Solution (5 mL/donor, STEMCELL Technologies) for 5 min at room temperature. Platelets were then removed by centrifugation (129 x g, 10 min, room temperature). The purified CD4$^+$ cells were minimally depleted of CD45RO$^+$ cells using half of the recommended concentration of EasySep Human Naïve CD4$^+$ T Cell Isolation Kit and Magnet (STEMCELL Technologies). Negative fraction from the magnetic isolation were stained with antibodies for 15 min at room temperature, and flow-sorted for naïve blood CD4$^+$ T cells (CD4$^+$CD25$^-$CD127$^+$CD45RA$^{hi}$CD45RO$^-$CD62L$^{hi}$) using FACSAria Fusion (BD Biosciences). Flow-sorted cells were frozen and thawed on the day of experiment.

### T cell expansion and polarization

For all polarization and IL2-based expansion experiments (Figures 3F, 3G, 7, S4B–S4D, and S7), T cells were incubated in normoxic conditions (20% $O_2$, 37°C, 5% $CO_2$), maintained at a concentration of 0.5 x $10^6$ cells/mL and cell density of 0.3 x $10^6$ cells/cm$^2$, and expanded in Immunocult-XF T Cell Expansion Media (STEMCELL Technologies) supplemented with 1X Pen/Strep (GIBCO) and 100 IU/mL IL-2 (Proleukin), and stimulated with 2.5% anti-CD2/3/28 (see below). For polarization experiments, the cells were further supplemented with the following polarization cocktails for the entirety of culture period. Th0 cocktail: no additional cytokines added; Th1 cocktail: 10 ng/mL IL-12, 1 μg/mL anti-IL-4; Th2 cocktail: 10 ng/mL IL-4, 1 μg/mL anti-IFNγ; and Th17 cocktail: 10 ng/mL IL-1β, 10 ng/mL IL-6, 20 ng/mL IL-23, 10 ng/mL TGF-β1, 5 μg/mL anti-IFNγ, and 5 μg/mL anti-IL-4.

On day 0, iPSC-, thymic-, or blood-CD4$^+$ T cells were stimulated with 2.5% anti-CD2/3/28 (STEMCELL Technologies). Cells were split every 2-3 days and replated at the above cell density/concentration, with cytokines replenished. iPSC- and thymic-CD4$^+$ T cells were restimulated on day 7 with 2.5% anti-CD2/3/28, and underwent an additional 7 days of expansion/polarization. On day 14 (iPSC- and thymic-CD4$^+$ T cells) or day 7 (blood-CD4$^+$ T cells), cells were collected, washed, and resuspended in fresh Immunocult-XF T Cell Expansion Media supplemented with only 10 IU/mL IL-2 (Proleukin), and rested for 16-24 hours prior to running downstream assays. Post-resting, cells were sampled, stained for relevant markers, and phenotyped on FACSymphony A5 (BD Biosciences).

### T cell proliferation, activation assay and intracellular cytokine staining

For proliferation assays (Figures 3F and S4E), sorted iPSC-CD4$^+$ T cells were expanded for 7 days using conditions listed above, then rested overnight in 10 IU/mL IL-2. Post-rested cells were washed twice with PBS, and stained with 10 μM Cell Proliferation Dye (CPD) eFluor$^{TM}$ 450 (Thermo Fisher Scientific) for 10 min at RT. Staining reaction is quenched by adding complete RPMI solution (RPMI supplemented with 10% Bovine Serum, 1% Pen/Strep, 1% GlutaMax) to stained cell mixture at a 1:5 v/v cell to complete RPMI ratio, for 5 min on ice. Cells are then spun down (500 x g, 5 minutes), washed with PBS, then plated at 50 x $10^3$ cells/200 μL in a 96-well flat-bottom, in Immunocult-XF T Cell Expansion Media supplemented with: 10 or 100 IU/mL IL-2, ±2.5% anti-CD2/3/28 complexes

(STEMCELL Technologies). Cells were incubated in normoxic conditions (5% $O_2$, 37°C, 5% $CO_2$) for 72 hours. Post-stimulation, cells were harvested, stained, and phenotyped on FACSymphony A5 (BD Biosciences).

For activation assays (Figures 3G and S4F), post-rested cells were washed twice with PBS, and plated at 100 x $10^3$ cells/200 μL in a 96-well flat-bottom, in Immunocult-XF T Cell Expansion Media supplemented with 10 IU/mL IL-2 and 2.5% anti-CD2/3/28 complexes (STEMCELL Technologies). Cells were incubated in normoxic conditions (5% $O_2$, 37°C, 5% $CO_2$) for 48 hours. Post-stimulation, cells were harvested, stained, and phenotyped for activation markers on FACSymphony A5 (BD Biosciences).

For intracellular cytokine secretion assays (Figures 7D and S7E), post-rested cells were washed twice with PBS, and plated at 50 x $10^3$ cells/200 μL in a 96-well round-bottom, in Immunocult-XF T Cell Expansion Media. Unstimulated cells were supplemented with 10 μg/mL Brefeldin A. Stimulated cells were supplemented with 10 μg/mL Brefeldin A, 10 ng/mL PMA, and 500 ng/mL ionomycin. Cells were incubated in normoxic conditions (5% $O_2$, 37°C, 5% $CO_2$) for 4 hours. Cells were then harvested, stained, and phenotyped on FACSymphony A5 (BD Biosciences).

### Flow cytometry

Antibodies can be found in "key resources table." HBSS or PBS supplemented with 2% FBS was used as Flow buffer. Staining was done entirely in 96-well V-bottom plates. Cells were collected and washed once with PBS. Cells were stained with Fc-blocking antibodies (BD Biosciences or Thermo Fisher) to reduce non-specific binding and Fixable Viability Dye (BioLegend or Thermo Fisher) to exclude dead cells. Cells were stained for surface proteins in PBS or Flow buffer for 30 min in the dark at 4°C or room temperature. Brilliant Plus Buffer was included in staining mixes when using at least three BV or BUV antibodies. Cells were washed with PBS or Flow buffer, resuspended in Flow buffer, and acquired on FACSymphony A5 (BD Biosciences) or CytoFLEX LX N3-V5-B3-Y5-R3-I0 (Beckman Coulter).

For detection of TFs in Figures 4E–4G, S5D, and S5E, cells were seeded into different TCR/Notch stimulation/inhibition conditions, collected at the indicated times, washed with PBS of Flow buffer, fixed and permeabilized with eBioscience Foxp3/Transcription Factor Staining Buffer Set (Thermo Fisher) for 45 min in the dark at room temperature or 4°C overnight, then stained for intracellular proteins for 45 min in the dark at 4°C or room temperature. Brilliant Plus Buffer was included in intracellular staining mixes when using at least three BV or BUV antibodies. Cells were washed and resuspended in Perm Buffer from the eBiosciences kit and acquired on the FACSymphony or CytoFLEX.

For detection of phosphorylated proteins in Figure 4D, cells were seeded into different TCR/Notch stimulation conditions in a reverse-timecourse, such that samples were stimulated at different times, then all collected simultaneously after the target timepoint was reached for all samples. At the target timepoint, cells (in 100 μL media in 96-wells) were quenched with 200 μL ice-cold PBS to slow down signaling reactions. Fixation/permeabilization was done with the BD Cytofix/Cytoperm™ Fixation/Permeabilization Kit (BD Biosciences). Cells were transferred to V-bottom wells, spun down for 2 min at 500 x g in a pre-chilled centrifuge (1°C), washed with 200 μL ice-cold PBS, spun down again, resuspended in 50 μL ice-cold PBS + Fc Block (BD Biosciences) and Zombie UV viability dye (BioLegend) for 5 min on ice in the dark, then finally fixed by adding 50 uL (1:1 volume) pre-warmed Cytofix™ Fix Buffer (BD Biosciences) and incubating for 15 min at 37°C. For permeabilization, cells were spun down for 5 min at 1000 x g, resuspended in 200 μL Perm/Wash Buffer I (BD Biosciences), and incubated in the dark at RT for 10 min. Cells were subsequently spun down again, washed once with 200 μL Perm/Wash Buffer I, spun down again, and stained with antibodies diluted in Perm/Wash Buffer I for 30 min in the dark at 4°C. Cells were washed and resuspended in Perm/Wash Buffer I and acquired on the CytoFLEX.

Data were analyzed on FlowJo software (v10; BD Biosciences) or CytExpert (v2.6; Beckman Coulter), then exported for plotting and statistical analysis with GraphPad Prism (v10, GraphPad Software) or Python (3.11.4).

Dose-response curves in Figures 1C and 1E were smoothed with a B-spline representation, with a uniform weight of $\mathbf{1}/\sigma$ applied ($\sigma$ = standard deviation of percents or yields per line), and smoothing factor $\boldsymbol{s}$ given by the number of points per line. The resulting spline curves were fit separately for each replicate and averaged to get the mean ± standard deviation for plotting the line ± shaded area.

### RT-qPCR

RNA was isolated using the Absolutely RNA Nanoprep Kit (Agilent) with minor modifications to the manufacturer's protocol. Briefly, 3 days after seeding iPSC-DP stage cells into SP induction conditions with 0.3% anti-CD2/3/28 on plates coated with 2.5 μg/mL VCAM1 ± 10 μg/mL Notch ligands, cells were harvested from their wells and washed once with 2% FBS in HBSS. Samples were pelleted at 500 x g for 5 minutes, resuspended in lysis buffer plus beta-mercaptoethanol (at 99.4uM final concentration), and stored at -80°C until RNA extraction. Later, lysates were thawed and transferred to RNA isolation columns, where they first treated with DNase and processed according to the manufacturer's protocol. Columns were warmed at 55°C prior to elution to increase RNA yield. cDNA was generated using the SuperScript IV VILO Master Mix (Invitrogen) according to the manufacturer's protocol. RNA inputs were normalized between samples for reverse transcription. Output cDNA samples were diluted, and 1 ng equivalent of RNA input was used per reaction for qPCR with 250 nM of each primer. qPCR was performed using the PowerUp SYBR Green Master Mix (Applied Biosystems) at 20 uL total reaction volume within the QuantStudio 6 Pro (Applied Biosystems), with 40 cycles and 60°C annealing temperature.

### Sample preparations for CITE-seq

For the PSC-DP T cells sequenced with CITE-seq and shown in Figures S1F and S1G, iPS11-derived Pro-T cells were generated in our standard conditions, then matured towards DP cells for two weeks in PSC2 media prior to collection on day M14 for sequencing (n=1).

For the PSC-SP T cells sequenced with CITE-seq + scTCRseq and shown in Figures 5, 6, and S6, iPS11-derived Pro-T cells were generated in our standard conditions, then matured towards DP cells for two weeks in PSC2 media. On DP maturation day M14, cells were collected and re-seeded 1:1 on wells coated with 10 μg/mL DLL4 + 2.5 μg/mL VCAM1 and in StemSpan T cell maturation media (SCT SFEM, STEMCELL Technologies) supplemented with 0.1% anti-CD2/3/28. On SP induction day S7, cells were again collected and re-seeded on fresh DLL4+VCAM1 in fresh SCT SFEM media containing 0.3% anti-CD2/3/28. On SP induction day S14, cells were collected and magnetically sorted for $CD3^+$ cells using the EasySep Release Human CD3 positive selection kit (STEMCELL Technologies) according to manufacturer's instructions. Cells were subsequently expanded by re-seeding 100 x $10^3$ cells/96-well on wells coated with 150 μg/mL RetroNectin (Takara Bio) + 3 μg/mL anti-CD3 (BioLegend) and in "PSC4" media[13] (JAC Ultra supplemented with 5 ng IL-7 + 5 ng IL-15, both from R&D Systems) further supplemented with 50 ng/mL IL-12 (BD Biosciences), 50 ng/mL IL-18 (R&D Systems), 20 ng/mL IL-21 (R&D Systems), 10 μM Z-VAD-FMK (R&D Systems), and 3 μg/mL anti-CD28 (BioLegend); see Table S7 for media formulations. After two days in these stimulation conditions (expansion day X2), cells were collected and re-seeded on wells coated only with 150 μg/mL RetroNectin and in PSC4 media without additional supplementation. Cells were fed with fresh media on expansion days X5 and X8, and collected for sequencing on expansion day X11 (n=1).

For CITE-seq antibody staining, the BioLegend TotalSeq-C CITE-seq antibody preparation and 10X Genomics CITE-seq cell staining protocols were followed. Briefly, one vial of TotalSeq-C Human Universal Antibody Cocktail v1.0 (BioLegend) was equilibrated to room temperature for 5 min and then spun at 10,000 x g for 30 seconds. The lyophilized panel was resuspended in 27.5 μL of HBSS + 4% FBS, vortexed for 10 seconds, and then incubated at room temperature for 5 minutes. The vial was vortexed again for 10 seconds and then spun at 10,000 x g for 30 seconds. The entire volume was transferred to a low protein binding PCR tube and then centrifuged at 14,000 x g for 10 min at 4°C.

Prior to CITE-seq antibody staining, 250,000 total cells were partitioned into a 12 x 75 mm tube. Cells were spun at 500 x g for 5 min at 4°C and resuspended directly in 12.5 μL of HBSS + 4% FBS. 12.5uL of the antibody staining cocktail was added and the cells were incubated for 30 min at 4°C. Cells were washed three times with 3.5 mL HBSS + 4% FBS and resuspended in a final volume of 55 μL. Cells were counted, stored on ice, and given immediately to the sequencing facility for 10X Genomics 5' library preparation and sequencing.

The generation of single cell indexed libraries was performed by the Biomedical Research Center Next Generation Sequencing Core using the 10X Genomics Chromium Controller platform and the Chromium Single Cell 5' Library and Gel Bead Kit v1.1 and Chromium Single Cell Library and Gel Bead Kit v2 reagents. The sequencing protocol provided by the supplier was followed without modification for CITE-seq and run with the NextSeq 2000. After run completion, the Binary base call (bcl) files were converted to fastq format using the Illumina bcl2fastq2 software, and data were received for further analysis.

### CITE-seq data processing and analysis

CellRanger (6.0.1) was used to align fastq files against the human genome (hg38) and quantify all single-cell samples. Muon (0.3.2) and Scanpy (1.10.4) in Python were used in the downstream analyses. Analysis notebooks are available on GitHub and archived on Zenodo: Figures S1F and S1G: https://github.com/stemcellbioengineering/stankiewicz-michaels-M14, https://doi.org/10.5281/zenodo.17861714; Figures 5, 6, and S6: https://github.com/stemcellbioengineering/jones-salim-cd4, https://doi.org/10.5281/zenodo.17861549.

RNA preprocessing involved filtering of empty cells, doublets, mitochondrial-high and ribosomal-high cells based on RNA counts. All thresholds were computed unbiasedly using 4 mean absolute deviations, with visual validation of the QC. After thresholding, we were left with 13285 cells (Figures S1F and S1G) and 5684 cells (Figures 5, 6, and S6).

Raw counts were first scaled to $10^4$ counts per cell using *sc.pp.normalize_total*, followed by $\log_2(x+1)$ transformation, and stored in the 'log1p' layer. Highly variable genes (HVGs) were identified using the default parameters of *sc.pp.highly_variable*. Principle components analysis (PCA) was performed on these HVGs with *sc.pp.pca* using the log1p layer and zero centering. The 50-dimension PCA was used to compute a *k*-nearest neighbours graph (k=20) which enabled Leiden clustering at varying resolutions for cell annotation purposes. In parallel, log1p counts were scaled with *sc.pp.scale* (Z-scored across cells) ± cell cycle regression and stored in separate layers ('log1p_zscore', 'ccreg'). log1p, log1p_zscore, and ccreg layers were all used to generate signature scores and visualizations to ensure consistency, with log1p_zscore results presented in the figures.

For the protein data, cells were not filtered based on protein expression, as cells with poor protein-capture quality could still contain valid mRNA profiles. We applied the centered log ratio transformation on the raw protein counts, followed by regression against six isotypes (adapted from Mulè et al.[67]) to adjust for background noise (Figures S6D and S6E). Finally, we applied ThresholdPy (0.1.5), our own Python implementation of ThresholdR,[68] to annotate proteins as expressed or unexpressed within cells using 2-component (more restrictive) or 3-component (less restrictive) Gaussian mixture models. Thresholded protein values were stored in layers 'prot_thresh2' or 'prot_thresh3' for the respective component numbers. Scaling was applied via *sc.pp.scale* (Z-scoring across cells) to generate the layers 'prot_thresh2_zscore' and 'prot_thresh3_zscore', the former of which was used for dotplots shown in Figure 5G.

### Signature gene collation and scoring

Signature gene sets were collected from prior human T cell development scRNAseq datasets (Chopp et al.[43] and Park et al.[69]) and from a study that compiled CD8$^+$ T cell functional signatures (Mazziotta et al.[66]). Any genes not captured in our dataset were filtered out. All signature gene sets we utilized and generated are available in Table S2).

For functional signatures (Mazziotta et al.[66]), we used the following: ''Naïve/CM-like'' (naïve/central memory), ''Tem'' (CD45RO+ effector memory), ''ISG'' (interferon signaling), ''Tmem/prolif'' (proliferating memory cells), ''NKL/Temra'' (NK-like/CD45RA+ EM), and ''Exhaustion''. The signatures were lightly modified to add *KLF2* to the ''Naïve/CM-like'' signature, and move *TOX* and *BATF* to the ''Exhaustion'' signature.

Chopp CD4/CD8: we collected pre-defined CD4 and CD8 signatures from Chopp et al.,[43] which were respectively defined from mouse and human cells based on differential expression of genes in CD4$^+$ and CD8$^+$ T cell clusters vs each other and DP T cell clusters (>1.5 $\log_2$ fold-change).

Park CD4/CD8: we created analogous signatures as above from CD4$^+$ and CD8$^+$ T cells in Park et al.[69] by finding genes with >1.5 $\log_2$ fold-change between all combinations of CD4$^+$ T cell clusters (''CD4+T'', ''CD4+Tmem'') vs CD8$^+$ T cell clusters (''CD8+T'', ''CD8+Tmem'') and DP cell clusters (''DP(Q)'', ''DP(P)''). These new CD4 and CD8 signatures contain 48 and 54 genes, respectively (see Table S2). Most genes were absent or very low in our dataset, so these signatures were only used in Figure S6B.

Schmiedel CD4/CD8: to better differentiate naïve CD4$^+$ vs CD8$^+$ T cells, we extracted all protein-coding genes with >2-fold change between naïve CD4$^+$ vs CD8$^+$ T cells in a bulk RNAseq dataset of sorted T cells.[107] These CD4 and CD8 signatures contain 28 and 34 genes, respectively (see Table S2). Most genes were absent or very low in our dataset, so these signatures were only used in Figure S6B.

Union CD4/CD8: To create more unified and robust signatures, we intersected the Chopp et al.[43] and Park et al.[69] datasets by compiling differentially-expressed genes (DEGs) in CD4$^+$ and CD8$^+$ T cell clusters in Chopp et al.[43] (''hs-ImCD4'', ''hs-MatCD4'', ''hs-ImCD8'', ''hs-MatCD8'', ''hs-CD8'') and Park et al.[69] (''CD4+T'', ''CD4+Tmem'', ''CD8+T'', ''CD8+Tmem''). As part of the processing, we excluded genes present in both the Union CD4 and CD8 signatures, genes present in the Mazziota et al.[66]-derived Naïve/CM-like signature above (due to many overlapping genes like *IL7R*, *SELL*, and *KLF2*), and the genes *CD8A*, *CD8B*, and *CD7* (to reduce circularity and non-specificity). The final Union CD4 and CD8 signatures contain 41 and 52 genes, respectively (see Table S2).

Jones CD4/CD8: Finally, to create more refined signatures that both ensure differential expression between CD4 and CD8 clusters and include essential genes often missed in the above signatures, we manually curated genes sets by first listing well-known CD4 T cell-associated genes (''Jones CD4 v1'' and ''Jones CD8''), then removing genes from the former that were expressed very lowly or not notably differentially expressed in ''CD4+T'' and ''CD4+Tmem'' clusters compared to ''CD8+T'' and ''CD8+Tmem'' clusters in Park et al.[69] Next, we added genes from the CD4- and CD8-associated cluster DEGs (see above) in both Park et al.[69] and Chopp et al.,[43] as well as the compiled CD4 signature gene set from Chopp et al.,[43] again filtering for those that were notably differentially expressed in CD4 vs CD8 Park et al.[69] and not naïve-associated (e.g. *IL7R*, *SELL*, *KLF2*). The final CD4 signature is called ''Jones CD4 v2'' in Table S2 and more annotated ''Jones CD4'' in figures.

Signature scores were calculated as $\mu_{Si} - \mu_C$, where $\mu_{Si}$ is the mean of scaled signature ***i*** genes and $\mu_C$ is the mean of scaled control genes. This scoring was based on a modified workflow using Scanpy's gene set scoring function (*sc.tl.score_genes*), which normalizes signature gene expression against a set of pseudo-randomly-selected control genes in a standard reference set.[108] The algorithm selects control genes based on the binned distribution of marker gene expression, averaged across all cells (25 bins, 50 control genes pseudo-randomly chosen per bin containing at least one marker gene). A fixed random number generator seed ensures repeatable selection of control genes. To create a uniform set of control genes that is applicable to all of our signatures, we first passed a list of all genes from all signatures into *sc.tl.score_genes* using the standard log1p expression layer, then collected the generated list of control genes. As log1p values do not give a sense of relative gene expression across cells/clusters, we computed signature scores with the log1p_zscore layer and manually subtracted the average of control genes from that of the *sc.tl.score_genes*-identified signature genes (on a per-cell basis). The overall scores are thus scaled signature gene means, corrected for scaled control gene expression per cell. The selection of control genes used log1p values due to suboptimality of the Z-scored values: the binning process in *sc.tl.score_genes* is based on ranked average gene expression across cells, which is definitionally zero for all genes when z-scored across cells. Signature scores and individual gene contributions to the scores for the heatmaps shown in Figures 5E, 5F, and S6B are given in Tables S3, S4, and S5, respectively.

### TCR repertoire analysis

Scirpy (0.22.0) was used to process scTCRseq data and collate unique primary TRA/TRB nucleotide sequences per cluster or gated SP subset. PSC-T cell scTCRseq data were compiled with fetal and postnatal thymocyte data[69] and PBMC data.[75] Thymocyte reference datasets:

- Fetal 13w: F38_TH_45P
- Fetal 14w: F30_Th_45P
- Fetal 17w: F29_TH_45P
- Postnatal 10m: T03_TH_TOT_1
- Postnatal 30m: T06_TH_TOT_1

As an unbiased estimator of TCR repertoire diversity, we used Simpson's Diversity ($D$). This was computed on TCR clones (unique productive rearrangements of CDR3, V, and J segments) separately for TCRα and β chains using the formula:

$$D = \frac{\sum_{i=1}^{R} n_i(n_i - 1)}{N(N - 1)}$$

where $R$ is the total number of TCR clones, $n_i$ is the number of templates for each clone $i$, and $N$ is the total number of TCR templates. The value $D$ is interpreted as the probability that two sampled templates are from the same TCR clone.[109] $D = 0$ indicates each sequencing template was sampled from a unique clone, while $D = 1$ indicates all templates were sampled from the same clone. In postnatal thymocyte samples that we evaluated,[69] the number of cells was in the 100's and no templates came from the same clone.

The variance ($D_{var}$) was approximated using a higher moment[77]:

$$D_{var} = \frac{a}{1 - b} \cdot D_T - \frac{b}{1 - b} \cdot D^2 + \frac{c}{1 - b} \cdot D$$

where

$$D_T = \frac{\sum_{i=1}^{R} n_i(n_i - 1)(n_i - 2)}{N(N - 1)(N - 2)}, a = \frac{4(N - 2)}{N(N - 1)}, b = \frac{2(2N - 3)}{N(N - 1)}, c = \frac{2}{N(N - 1)}$$

For plotting, we show $D \pm D_\sigma$, with the standard deviation estimated as $D_\sigma = \sqrt{D_{var}}$.

Segment usage densities smoothing was done with a B-spline representation, with a uniform weight of $1/\sigma$ applied ($\sigma$ = standard deviation of segment usage frequencies), and smoothing factor $s$ given by the number of segments per V or J array.

## QUANTIFICATION AND STATISTICAL ANALYSIS

For all *in vitro* experiments, two-tailed Student's T tests or one-, two-, or three-way ANOVA were used to determine statistical significance. For T tests, one-way ANOVA, and ANOVA HSD post-hoc tests, $P < \alpha = 0.05$ was considered significant; for multi-way ANOVA, $P < \alpha = 0.01$ was considered significant. Values for n represent independent differentiations of iPSCs-derived HSPCs or HE cells to downstream cell types, and are provided in figure legends. Definitions of center, error bars, and confidence intervals are also provided in figure legends.

### Multi-way ANOVA

The Python package statsmodels (v0.14.0) was used for multi-way ANOVA modeling. Each population percent, cell type yield, or log-transformed geomean value was fit with an ordinary least squares model of the form:

$$y \sim X_1 \times X_2 \times \ldots \times X_n + \epsilon$$

Where $y$ is the measured value and is modeled as a full-factorial function of different variables $X_i$ and residual error $\epsilon$. Hypotheses were tested with Type II sum-of-squares. A threshold of p = 0.01 was considered significant. Detailed statistics for all ANOVA calculations are provided in Table S1.